New Late Cretaceous and Paleogene paleomagnetic results from south China and their geodynamic implications

Zhiming Sun,[1] Zhenyu Yang,[2] Tienshui Yang,[3] Junling Pei,[1] and Qinfan Yu[4]

Received 28 September 2004; revised 5 November 2005; accepted 22 November 2005; published 4 March 2006.

[1] To better understand the tectonic evolution of South China Block (SCB) in response to the India-Asia collision, we present new paleomagnetic results from Late Cretaceous and Paleogene red bed formations of the Hengyang basin of Hunan province, in the interior part of the SCB. Stepwise thermal demagnetization of the rocks isolated a high-temperature component. The tilt-corrected mean direction from the Late Cretaceous rocks is D = 15.6°, I = 29.9° with a_{95} = 5.7°, N = 26 sites, corresponding to a paleopole at 71.9°N, 236.3°E with A_{95} = 4.7°, which passes reversal tests. The tilt-corrected mean direction (D = 358.9°, I = 35.4° with a_{95} = 5.0°, N = 22 sites) from the Paleogene rock, which passes the reversal test, gives a pole at 82.6°N, 300.6°E with A_{95} = 4.4°. The low-field anisotropy of magnetic susceptibility results suggest that the red beds have not experienced significant strain due to compaction or tectonic stress, while the anisotropy of isothermal remanence results suggest that postdepositional compaction in these red beds produced no more than 3°–4° of inclination shallowing. These paleomagnetic and rock magnetic tests imply that the remanence is primary. On the basis of paleomagnetic results obtained from coeval basalts in Mongolia and Siberia, we suggest that no significant latitudinal motion has taken place between the SCB and Siberia since the Late Cretaceous. The significant latitudinal discrepancy between the SCB and European block could be due to nonrigid behavior of the Eurasian plate since the Late Cretaceous. A 16.7 ± 5.0° clockwise rotation of the SCB during the Late Cretaceous to the Paleogene could be related to the collision of India and Asia in the west and the subduction of the circum-Pacific plate to eastern Asia in the east.

Citation: Sun, Z., Z. Yang, T. Yang, J. Pei, and Q. Yu (2006), New Late Cretaceous and Paleogene paleomagnetic results from south China and their geodynamic implications, *J. Geophys. Res.*, *111*, B03101, doi:10.1029/2004JB003455.

1. Introduction

[2] South China is divided into the Yangtzi Craton to the northwest and the south China fold belt system to the southeast (Figure 1). A large number of reliable paleomagnetic data suggest that the collision between the North China Block (NCB) and South China Block (SCB) started in the latest Permian and Early Triassic near the Dabie fold belt and that the final suturing was complete by no later than the late Jurassic. These Chinese blocks are assumed to have been fully assembled with Eurasia and to have suffered no relative latitudinal movement by the Early Cretaceous [*Zheng et al.*, 1991; *Huang and Opdyke*, 1992; *Gilder and Courtillot*, 1997; *Yang and Besse*, 2001]. However, many local or regional vertical axis rotations have occurred in the SCB since the Cretaceous [*Enkin et al.*, 1991; *Gilder et al.*, 1993; *Huang and Opdyke*, 1992; *Otofuji et al.*, 1998]. Because of either the collision beginning at 55 Ma between India and Asia in the west [*Dewey et al.*, 1989] or the subduction of the circum-Pacific plate beneath the Asian continental margin in the east since the Early Cretaceous, the SCB may have suffered from significant intercontinental deformation and block rotations. According to the extrusion model [*Tapponnier et al.*, 1982], for example, Indochina was first moved largely to the southeast along the Red River fault zone relative to the SCB, accompanied by 20°–25° clockwise rotation. Subsequently, the SCB should have moved eastward and rotated with respect to the NCB along the Qinling fault belt since the Neogene. The former has been studied intensively through paleomagnetic method [*Yang and Besse*, 1993; *Sato et al.*, 2001].

[3] Previous paleomagnetic studies of the Late Cretaceous in the SCB mainly concentrated on the continental margin of the SCB (the western Sichuan and coastal provinces) [*Enkin et al.*, 1991; *Gilder et al.*, 1993; *Chan*, 1991; *Huang and Opdyke*, 1992] (Figure 1). These paleomagnetic poles from the continental margin show generally a distribution along a small circle centered in the sampling areas, indicating either the local deformations due to the influence of strike-slip faults zones such as the Xianshuihe-Xiaojiang fault system, the Red River fault system, or the Changle-Nanou fault zone. In other

[1]Laboratory of Paleomagnetism, Institute of Geomechanics, Chinese Academy of Geological Sciences, Beijing, China.
[2]Department of Earth Sciences, Nanjing University, Nanjing, China.
[3]Institute of Tibetan Plateau Research, Chinese Academy of Science, Beijing, China.
[4]Department of Geophysics and Geoinformation Systems, China University of Geosciences, Beijing, China.

0148-0227/06/2004JB003455$09.00

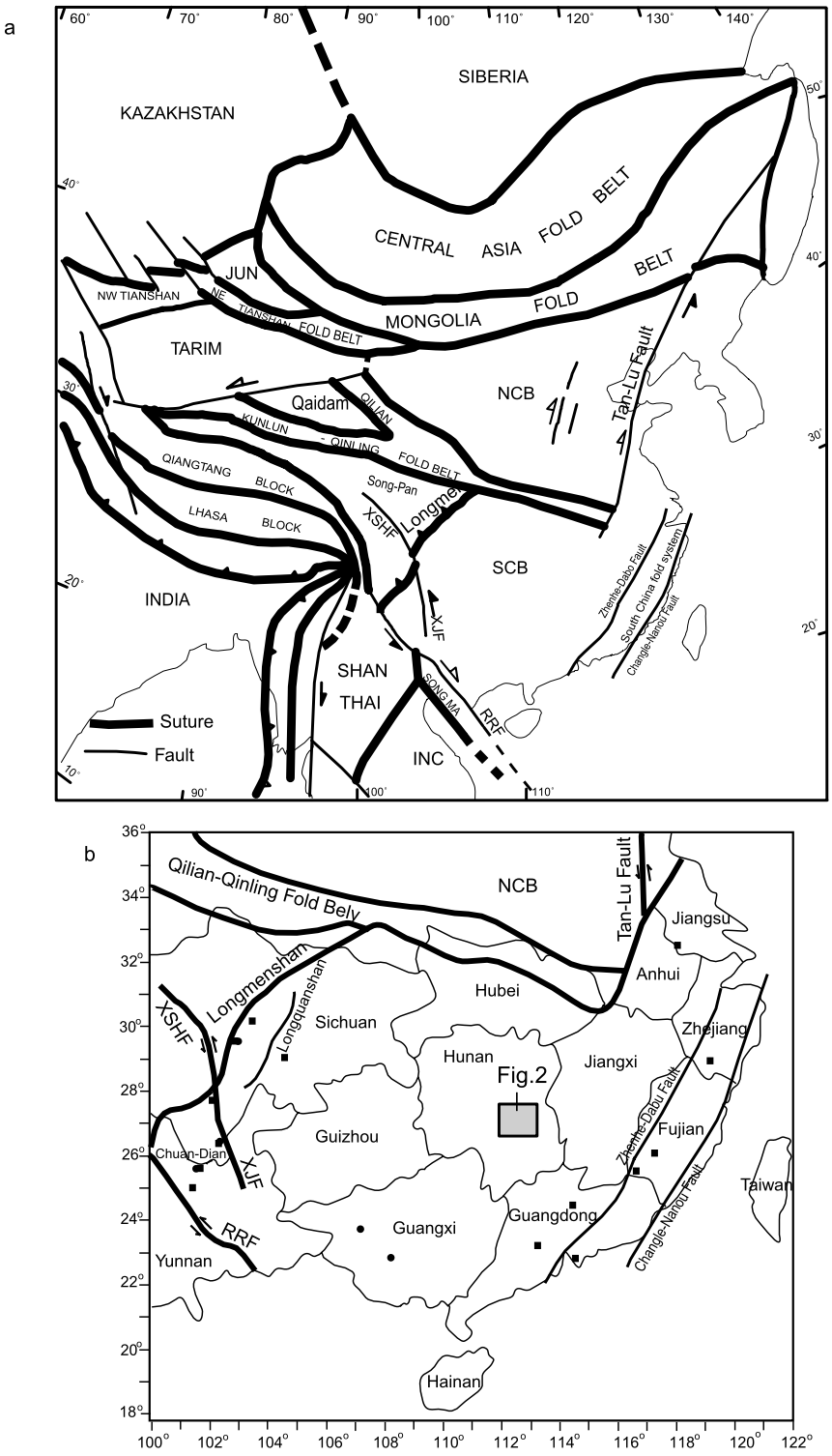

Figure 1. (a) Simplified tectonic map of China and adjacent area showing the main sutures and faults. (b) Regional geologic map of south China [after *Gilder et al.*, 1993]. The major blocks are Kazakhstan, Siberia, Mongolia, JUN (Junggar), NCB (North China Block), Qaidam, Tarim, Kunlun, Qiangtang, SCB (South China Block), INC (Indochina), India, Lhasa. RRF, Red River Fault; XSHF, Xian Shui He Fault; XJF, Xiao Jiang Fault. Solid squares (circles) indicate location of published paleomagnetic sites in Late Cretaceous (Paleogene) rocks in SCB; shaded square indicates sampling area of Figure 2.

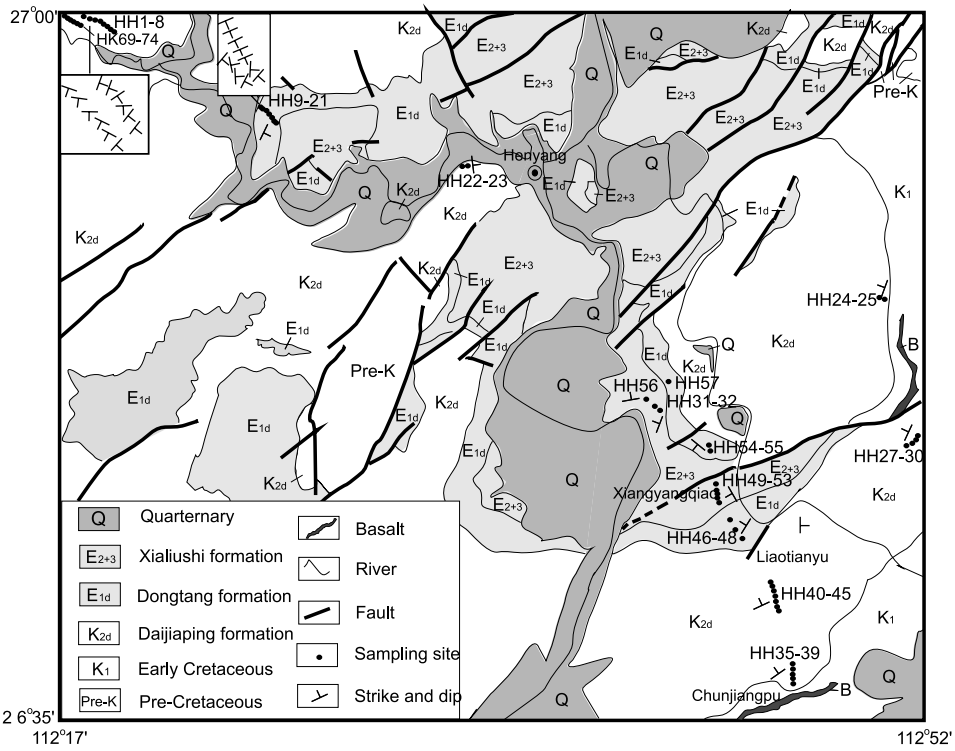

Figure 2. Geological map of Hengyang area showing the localities of Late Cretaceous and Paleogene sites (modified from *HBGMR* [1992]).

hand, a few Cenozoic paleomagnetic results are available with limited number of sites and samples. For example, *Huang and Opdyke* [1992] reported preliminary paleomagnetic results from 36 samples (seven sites) of the early Tertiary rocks in western Sichuan province. The early Tertiary poles reported by *Zhao et al.* [1994] and *Gilder et al.* [1993] were derived from 35 samples (five sites) and 17 samples (only one site), respectively, at a close area from Guangxi province (Figure 1). Previous studies also indicated that the Cretaceous paleolatitude of western Sichuan was significantly lower than that predicted by the poles of ''stable'' Eurasia [*Enkin et al.*, 1991; *Huang and Opdyke*, 1992], the discrepancy was resulted either from the northward shortening in the Qinling fold belt during the Tertiary or from errors in the reference apparent polar wander path (APWP) of Eurasia [*Enkin et al.*, 1991].

[4] Furthermore, a significant shallowing of paleomagnetic inclinations has been observed for Cretaceous and Tertiary paleomagnetic data in central Asia when compared with inclinations calculated from the reference poles of the stable Eurasian plate [*Besse and Courtillot*, 1991, 2002], which might imply a large continental shortening. However, this is in conflict with geological observations in the northern fold belts of the Tibetan Plateau and with topographic constraints [*Cogné et al.*, 1999]. Several hypotheses were proposed to explain this inconsistency, mainly including synsedimentary or compaction-induced inclination shallowing, tectonic shortening, nondipole field, or a poorly constrained APWP for Eurasia and nonrigidity of the huge Eurasian plate [*Thomas et al.*, 1993; *Halim et al.*, 1998; *Cogné et al.*, 1999; *Si and Van der Voo*, 2001; *Gilder et al.*, 2001, 2003; *Tan et al.*, 2003].

[5] To better understand the tectonic evolution of the SCB and Asian geodynamics since the Late Cretaceous, we carried out a paleomagnetic study on the Late Cretaceous and Paleogene red beds from the Hengyang basin (Hunan province) of the SCB. The studying areas are far away from the deformed continental margin of the SCB and are characterized by a relative low sedimentation rate that differs from the high sedimentation rate and energy of central Asian sites.

2. Paleomagnetic Sampling and Laboratory Technique

[6] Figure 1 shows the investigated basin located at the interior part of the SCB, where we sampled the Late Cretaceous and Paleogene red beds along a road near Hengyang city (26.9°N, 112.6°E). The Hengyang basin is one of the largest red bed basins in the SCB. Red beds were deposited continuously from the Early Cretaceous until the early Tertiary (Figure 2), which include the Early Cretaceous Shenhuangshan Formation, the Late Cretaceous Daijiaping Formation, the early Tertiary Dongtang and Xialiushi formations. The Cretaceous to Tertiary formations show weak deformation, with folding about a NE trending axis (Figure 2).

[7] The age of folding is considered as late Tertiary [*Hunan Bureau of Geology and Mineral Resources* (*HBGMR*), 1992]. The Daijiaping Formation consists mostly of red sandstones and siltstones. Fossils identified in this formation include Ostracoda (*Cristocypriden, Cypridea,* and *Harbinia*) and Charophyte (*Porochara*), indicative of Late Cretaceous time [*HBGMR*, 1992]. The Late Cretaceous age of the Daijiaping Formation is also supported by

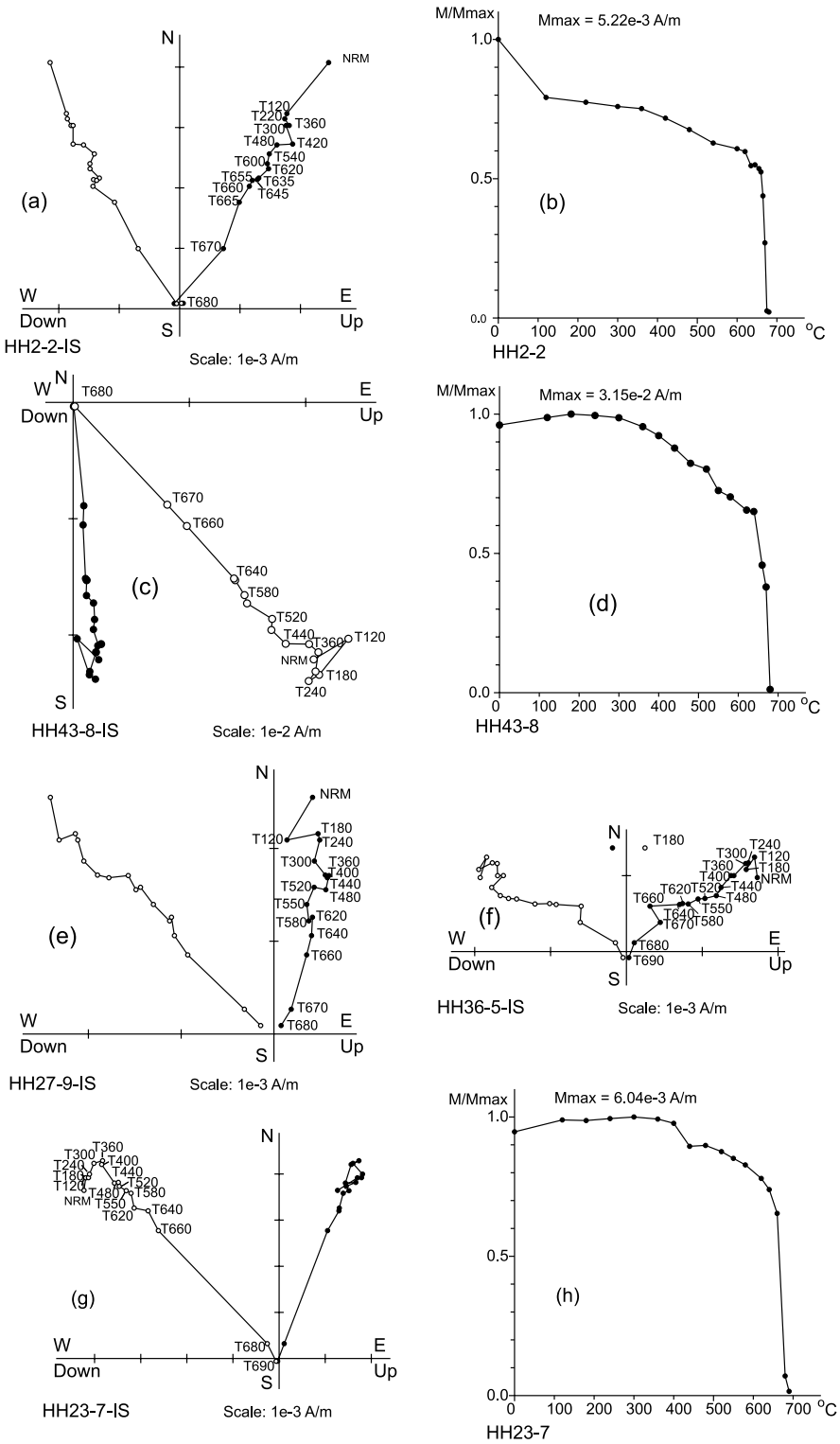

Figure 3. Representative Zijderveld diagrams and normalized intensity curves of thermal demagnetizations of NRM from Late Cretaceous samples. Almost all samples had an intensity drop at 680°C, which clearly indicates the presence of hematite. Solid (open) symbols refer to the projection on the horizontal (vertical) plane in situ coordinates. T200 = 200°C.

an Ar-Ar dating of the intercalated basalt flow (40 m) (85 Ma [*Ge et al.*, 1994]). The Paleogene Dongtang and Xialiushi formations (Figure 2 and Table 2), which consist mainly of red or purplish red, fine- to coarse-grained sandstones and siltstones. The fossils of Ostracoda (*Sinocypris, Funingensis, Jlyocypris, Changzhouensis*) and Charophyte (*Peckichara*) have been found in the Xialiushi Formation, indicative of Eocene time (54.8–33.7 Ma) [*HBGMR*, 1992]. On the basis of a preliminary magnetostratigraphic study of the Cretaceous-Paleogene sediments from the Hengyang

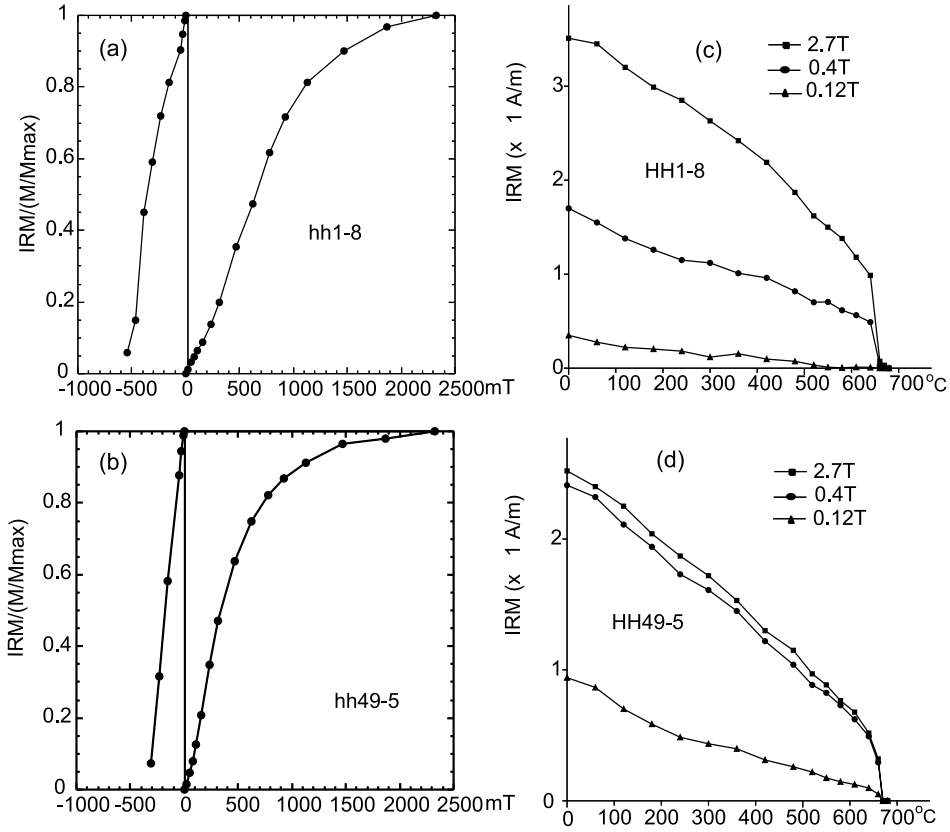

Figure 4. (a and b) Normalized isothermal remanent magnetization acquisition curves of red sandstone samples and opposite field demagnetization. (c and d) Three-component IRM thermal demagnetization showing unblocking temperatures around 680°C. Triangles, circles, and squares indicate soft (0.12 T), medium (0.4 T), and hard component (2.7 T) (Late Cretaceous sample (Figures 4b and 4d); Paleogene sample (Figures 4b and 4d)).

basin, the sequence of magnetic polarities recorded in the Daijiaping Formation can be corresponded to the polarity sequence of the Campanian and Maastrichtian stages. The sequence of magnetic polarities recorded in the Dongtang Formation can be correlated with polarity record of the Danian, and the sequence of magnetic polarities recorded in the Xialiushi Formation shows a general correspondence with the Danian and Thanetian stages. Therefore the age of the Daijiaping Formation is regarded as Late Cretaceous, while the Dongtang and Xialiushi formations are Paleocene in age (65–54.8 Ma) [*Ge et al.*, 1994]. Thus the fossils assemblages and magnetostratigraphic study give an age constraint of the Paleocene to Eocene (65–33.7 Ma) for the Xialiushi and Dongtang formations.

[8] We have sampled a total of 57 paleomagnetic sites in the Hengyang basin, which includes 31 Late Cretaceous sites and 26 Paleogene sites (Figure 2). Unfortunately, the basaltic flow intercalated in the upper part of the Dajiaping Formation is too thin and weathered to collect paleomagnetic samples. Eight to ten core samples distributed over several meters were drilled at each site with a gas-powered drill and were orientated with a magnetic compass. Core samples were cut into 2.3-cm-long cylinders for subsequent paleomagnetic analysis. All samples were subjected to progressive thermally demagnetization in 17–21 steps in an ASC TD-48 oven with an internal residual field lower than 10 nT, and measured with a 2G cryogenic magnetometer inside a set of large Helmholtz coils that reduced the ambient geomagnetic field to around 300 nT at the paleomagnetic laboratory of the Institute of Geomechanics in Beijing. Magnetization directions were determined by principal component analysis [*Kirschvink*, 1980]. The site-mean of paleomagnetic directions was calculated using *Fisher* [1953] statistics.

[9] Some representative samples were selected for acquisition and direct field demagnetization of isothermal remanent magnetization (IRM) to examine their mineralogical carriers. We have also used the thermal demagnetization of IRM successively applied in different filed and along three orthogonal axes of a sample as described by *Lowrie* [1990]. The samples were magnetized in sequence along their Z, Y, and X axes with fields of 2.7, 0.4, and 0.12 T, respectively. The composite IRM was then thermally demagnetized up to 675°C.

[10] We also selected 85 (Late Cretaceous) and 40 (Paleogene) samples to measure the anisotropy of magnetic susceptibility (AMS) and the anisotropy of isothermal remanence (AIR), respectively.

3. Paleomagnetic Results

3.1. Late Cretaceous Daijiaping Formation

[11] Figure 3 shows a representative Zijderveld plot and normalized intensity curves. Most samples possess two

Table 1. Paleomagnetic Results From the Late Cretaceous Daijiaping Formation in Hengyang Basin (26.9°N, 112.9°E), Hunan Province, South China[a]

Site	Slat	Slon	Strike	Dip	N(n)	D_g	I_g	D_s	I_s	κ	α_{95}	Plat	Plon	A_{95}
hh1	27.0	112.3	20	7	6/7	19.8	27	23.7	26.1	38.6	10.9	64.2	228.5	8.7
hh2	27.0	112.3	20	7	8/8	16.5	32.6	21.6	32.1	41.4	8.7	67.9	223.5	7.4
hh3	27.0	112.3	56	11	5/8	22.3	27.2	27.9	32.5	143.3	6.4	62.6	216.4	5.4
hh5	27.0	112.3	88	14	7/7	24.2	1.1	25	13.3	17.9	14.7	58.8	238.2	10.7
hh6	27.0	112.3	38	12	9/9	6.3	27.7	12.6	33	15.1	13.7	62.9	237.5	11.7
hh7	27.0	112.3	38	12	7/8	21.4	32	28.1	34.1	17	15.1	75.3	214.2	13.1
hh22[b]	26.9	112.6	356	11	3/4	351.4	40.4	0.7	39.9	13.4	35.1	85.7	283.9	32.7
hh23[b]	26.9	112.6	353	10	4/5	354.4	42.4	3.3	41	15.4	24.2	85.5	250.7	22.9
hh24	26.8	112.	200	19	6/8	36.5	29.6	24.9	34	46.2	10	65.7	217.2	8.6
hh25	26.8	112.8	225	10	5/7	23.5	40.9	16.1	37	34	13.3	74	222.1	11.9
hh27	26.7	112.9	252	13	9/9	7.8	34	4.6	22.3	18.2	12.4	74.3	276	9.6
hh28	26.7	112.9	205	9.5	7/9	0	31.2	355.2	27.1	38.5	9.8	76.9	313.8	7.9
hh29	26.7	112.9	194	19	7/8	347.7	36.4	337.3	27	21.3	13.4	65.4	357.1	10.7
hh30	26.7	112.9	194	19	3/9	28.5	21.7	20.3	26	32.5	22	67	233.3	17.5
hh35	26.6	112.8	240	13	6/8	193.2	−36.9	187.6	−27.4	20	15.3	76	260.9	12.3
hh36	26.6	112.8	249	14	6/8	35.6	34.7	28.7	26.7	27.4	13	60.4	222.1	10.4
hh37	26.6	112.8	247	13	8/8	43.7	33.2	36.6	27.8	35.5	9.4	53.9	214.5	7.6
hh38	26.6	112.8	235	21	5/8	354.7	50.7	356.4	38.8	24.3	15.9	84.3	328.5	14.6
hh39	26.6	112.8	235	21	8/8	22	34.3	12.7	22	28.3	10.6	70.7	252.2	8.1
hh40	26.6	112.8	244	21	8/8	24.2	46.3	11.7	31.7	69	6.7	75.6	241.5	5.6
hh41[b]	26.6	112.8	240	14	4/8	216.2	−30.9	209.4	−25	12.2	27.5	59.4	223.1	21.7
hh42	26.6	112.8	245	18	7/7	203.6	−33.5	196.5	−21.5	39.1	9.8	68.1	244.5	7.5
hh43	26.6	112.8	249	15	7/7	183.7	−45.6	179	−31.9	19.3	14.1	80.6	298.7	11.9
hh44	26.6	112.8	255	15	5/7	351.1	22.6	350.6	7.7	34.5	13.2	65.6	316	9.4
hh45[b]	26.6	112.8	230	16	7/8	209.1	−48.1	194.8	−41.1	9.1	21.1	76.3	212.3	20
hk69	27.0	112.3	109.6	11.7	8/8	34.4	29.4	37	40.5	25	11.3	56.4	200.6	10.6
hk70	27.0	112.3	98	12	6/6	28.8	27.9	32.1	38.8	22.3	14.5	60.4	205.1	13.3
hk71	27.0	112.3	91	6	6/7	7.2	32.3	7.9	38.2	21.5	14.8	80.9	238.1	13.5
hk72[b]	27.0	112.3	116	8	6/7	43.1	22.8	44.5	30.4	15.9	17.3	47.5	207.4	14.4
hk73	27.0	112.3	118	10	7/8	29.1	20.7	29.4	30.7	22.8	12.9	60.9	217.2	10.7
hk74	27.0	112.3	42	5	8/8	27.9	21.7	29.9	22.6	22.4	12	58.1	225	9.3
Mean					26	18.3	32.4	-	-	22.1	5.7	-	-	-
								15.6	29.9	27.1	5.7	71.9	236.3	4.7

[a]Slat (Plat), latitude of site (pole); Slon (Plon), longitude of site (pole); N/n, number of samples used to calculate mean and measured; D_g, I_g, D_s, I_s, declination and inclination in geographic and stratigraphic coordinates, respectively; κ, the best estimate of the precision parameter; α_{95}(A_{95}), the radius that the mean direction (pole) lies within 95% confidence. Unit, degree.

[b]The data with $\alpha_{95} > 16°$ were not used to calculate the mean direction.

magnetic components: A low-temperature component (LTC; generally below 360°C) is aligned close to the present field, while a high-temperature component (HTC; 360°–680°C) trends toward the origin. The high unblocking temperature (680°C) of the Daijiaping Formation samples implies the presence of hematite, which is also confirmed by IRM acquisition and subsequent thermal demagnetization (Figures 4a and 4c). The IRM acquisition curve of the Late Cretaceous red beds (Figure 4a) reveals a rapid increase at first below a field of 1000 mT but does not reach saturation even in 2.7 T. Moreover, thermal demagnetization of the soft component (<0.12 T) shows an unblocking temperature at around 580°C, indicative of magnetite. The hard (0.4–2.7 T) and medium (0.12–0.4 T) components show a distinct unblocking temperature at 680°C, indicative of hematite. These results suggest that the Late Cretaceous red beds contain at least two magnetic minerals of magnetite and hematite. The Daijiaping Formation samples are therefore dominated by magnetite and hematite. The Late Cretaceous HTC data are listed in Table 1. The unfolding process reveals that the site-mean mean direction after tilt correction gives a maximum grouping of direction at about 71% unfolding (with uncertainties ranging from 52.9 to 89.1%) (D = 16.7°, I = 31.2°, a_{95} = 5.4°) [*Watson and Enkin*, 1993], which is statistically indistinguishable from that of 100% unfolding (D = 15.6°, I = 29.9°, a_{95} = 5.7°) (Figure 5). The gentle bedding attitudes of the Late Cretaceous red beds do not allow the fold test to be applied with any significance. The reversal test is positive at the 95% confidence level [*McFadden and McElhinny*, 1990] (Table 1). Besides, the results of magnetic polarity sequence from the Late Cretaceous red beds indicate that normal and reversal polarities are alternated within continuous stratigraphic level (Table 1). Thus we consider that the HTC of Daijiaping Formation at 100% unfolding may represent the primary remanence acquired during the sedimentation.

3.2. Paleogene Dongtang and Xialiushi Formations

[12] Similarly, thermal demagnetization also isolated two components of magnetization from the Paleogene Dongtang and Xialiushi formations. The directions of the LTC in the initial demagnetization steps (to 360°C) generally cluster around the present geomagnetic field, while a high unblocking temperature component was isolated between 360°C and 680°C (Figure 6 and Table 2). However, only a very few samples (HH54-4) show two different remanence components with blocking temperatures above 600°C. The remanence component between 630°–660°C may be a high-temperature overprint, or secondary chemical remanence. The HTC is of normal polarity at 9 sites and reversed polarity at 17 sites. The character of

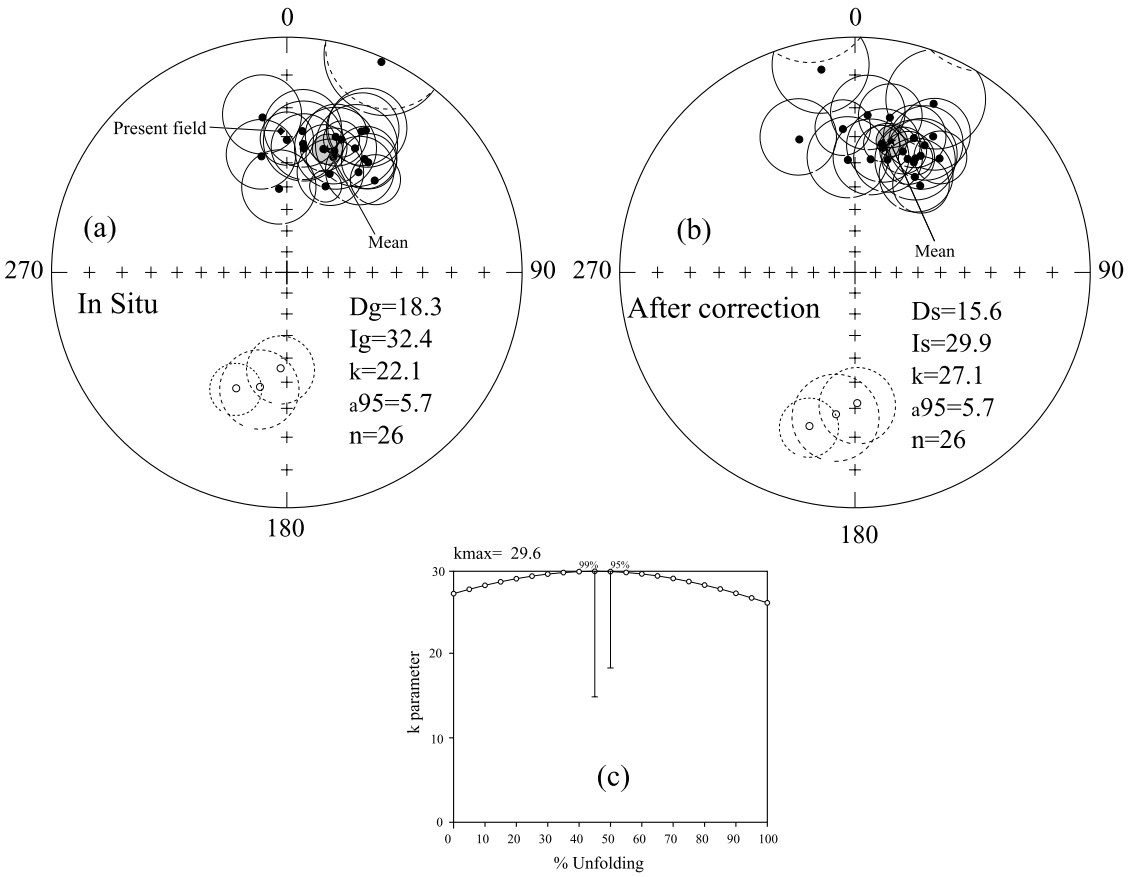

Figure 5. Equal-area stereographic projection of high-temperature component from Late Cretaceous formation in (a) geographic and (b) stratigraphic coordinates, respectively. Lower (upper) hemisphere directions are marked with closed (open) symbols. (c) Progressive unfolding of the mean direction showing a maximum concentration at 71% unfolding, which is not significantly different from that at 100% unfolding.

magnetic polarity from the Paleogene red beds is similar to that of the Late Cretaceous, showing that normal and reversal polarities are alternated within a continuous stratigraphic level (Table 2). The reversal test is positive at 95% confidence, and the *Watson and Enkin* [1993] test gives a maximum grouping of directions at 97% unfolding (with uncertainties ranging from 63 to 128.4%) (Table 2 and Figure 7). These results suggest that the HTC represents a primary magnetic remanence acquired during the Paleogene. The average site-mean direction before tilt correction is D = 358.4°, I = 32.1°, a_{95} = 6.2°, and D = 358.9°, I = 35.4°, a_{95} = 5.0° after tilt correction. The IRM acquisition of rocks from the Paleogene Dongtang and Xialiushi formations is similar to that of the Late Cretaceous red beds (Figure 4b). However, thermal demagnetization curves of a composite IRM show an unblocking temperature around 680°C, indicative of hematite (Figure 4d). The soft (<0.12 T) and medium (0.12–0.4 T) components with unblocking temperature (680°C) may suggest the presence of a different grain size of hematite family with different coercivities [*Robert et al.*, 1995]. Hematite with large grain sizes would correspond to the medium coercivity and part of the low-coercivity components, fine-grained hematite would correspond to the hard fraction. The rock magnetic experimental result of IRM acquisition and its thermal demagnetization indicated that hematite is the main carrier of the remanence.

4. Magnetic Anisotropy

4.1. Anisotropy of Magnetic Susceptibility

[13] It has been suggested that sediment compaction could have significantly reduced the inclination of remanence in red beds [*Ojha et al.*, 2000]. Compaction-induced inclination shallowing has also been observed in laboratory compaction experiments of fine-grained magnetite-bearing sediments [*Kodama and Sun*, 1992]. However, no significant inclination shallowing has been observed during laboratory compaction of coarse-grained hematite-bearing sediments [*Tan et al.*, 1996]. It is important to test whether sediment compaction could caused significant inclination shallowing of the remanence of the red beds in the Hengyang basin.

[14] We performed anisotropy of magnetic susceptibility measurements on 55 samples of the Late Cretaceous and 30 samples of the Paleogene from different sites using a Kappa bridge KLY-3 apparatus. The direction of the principal maximum (κ1), intermediate (κ2) and minimum (κ3) ellipsoid axes of the Late Cretaceous and Paleogene red beds are shown in Figures 8a and 8c, respectively. Although κ1

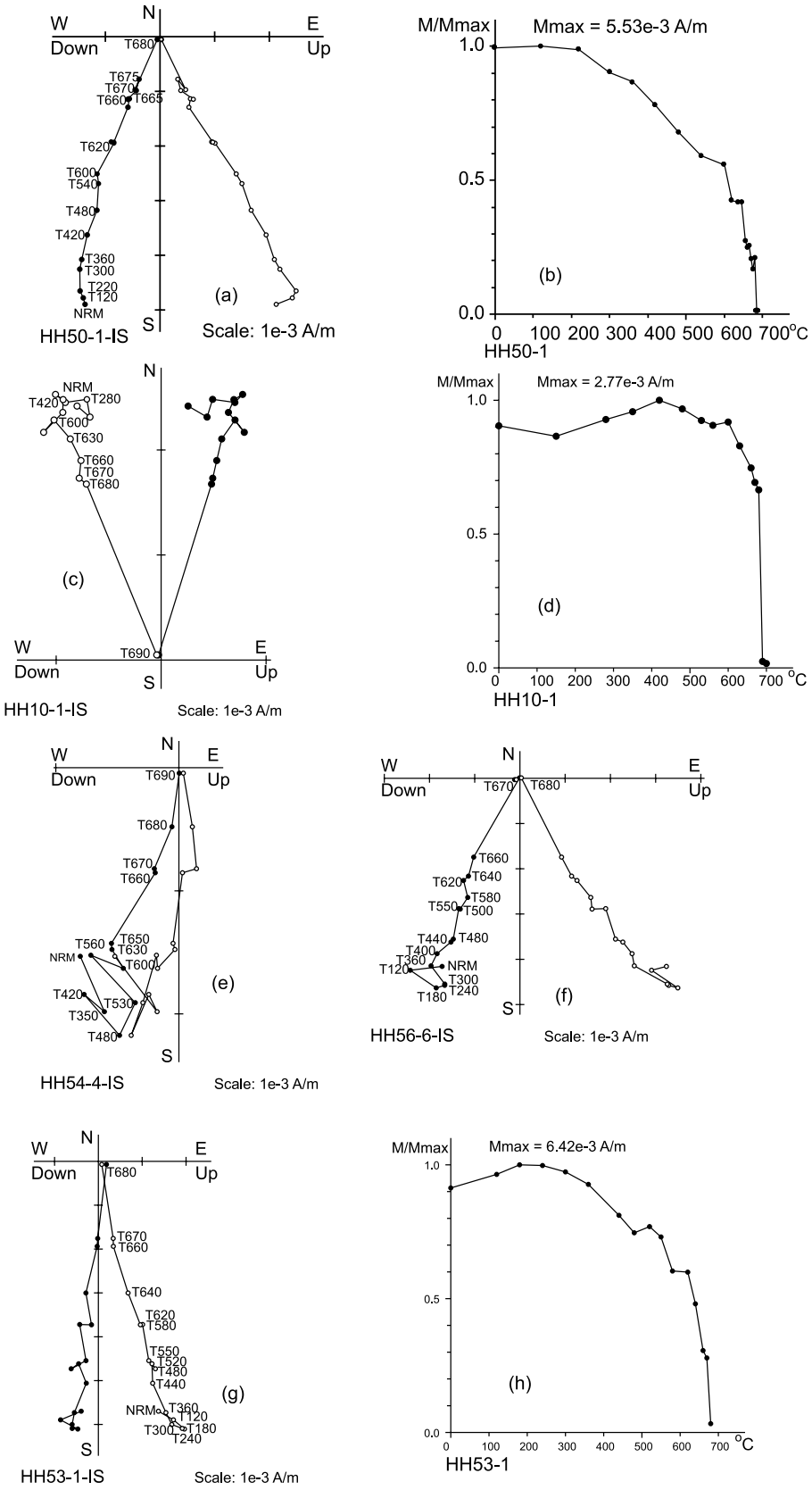

Figure 6. Representative Zijderveld diagrams and normalized intensity curves of thermal demagnetizations of NRM from Paleogene samples. Almost all samples had an intensity drop at 680°C, which clearly indicates the presence of hematite. Solid (open) symbols refer to the projection on the horizontal (vertical) plane in in situ coordinates. T200 = 200°C.

Table 2. Paleomagnetic Results From the Paleogene Dongtang and Xialiushi Formations in Hengyang Basin (26.9°N, 112.9°E), Hunan Province, South China[a]

Site	Slat	Slon	Strike	Dip	N(n)	D_g	I_g	D_s	I_s	κ	α_{95}	Plat	Plon	A_{95}
Dongtang Formation														
hh9	27.0	112.4	67	11	6/6	174	−33.4	177.1	−43.6	56.2	9	87	353.2	8.9
hh10	27.0	112.4	67	11	7/9	−1.1	13.5	0.5	23.5	29.6	11.3	75.3	290.4	8.8
hh11[b]	27.0	112.4	67	11	7/9	355	29.6	−2.1	39.8	13.2	17.3	85.2	316.2	16.1
hh12	27.0	112.4	64	9	5/7	169.5	−32.1	171.7	−40.6	40.9	12.1	81.6	357.3	11.4
hh13	27.0	112.4	64	9	6/8	159.8	−46.4	161.6	−55.3	39	10.9	72	56.3	13.1
hh14	27.0	112.4	40	7	7/8	175.7	−34.2	179.7	−38.7	38.4	9.9	84.8	295.4	9.1
hh15	27.0	112.4	348	12	5/6	343.8	11.2	346.3	11.4	56.1	10.3	65.1	326.3	7.4
hh16	27.0	112.4	357	5	8/8	169.3	−37.4	173.2	−37.7	16.1	14.3	81.5	340.3	12.9
hh17	27.0	112.4	27	5	8/8	340	43.7	343.7	47.1	47.8	8.1	75.5	31.1	8.4
hh18	27.0	112.4	3	12	8/8	2.7	48.7	15.8	46.8	18.1	13.4	76	194.4	13.9
hh19	27.0	112.4	41	9	8/8	181.6	−37	187.8	−42	45.7	8.3	82.4	222	9
hh20	27.0	112.4	8	7	6/8	356.2	21.7	−1	22.7	23.8	14	74.8	296	10.8
hh21	27.0	112.4	8	7	8/9	172.3	−34.1	177	−35.5	25.2	11.3	82.1	313.4	9.9
hh46	26.7	112.8	214	10	8/8	20.8	37.8	13.6	35.3	14	15.3	75.6	229.9	13.4
hh47	26.7	112.8	222	11	7/7	25.1	28.8	20	24.7	22.2	13.1	66.8	235.2	10.3
hh48	26.7	112.8	222	14	6/7	11.1	42.1	1.8	34.4	21.4	14.8	82	280.4	12.8
hh54	26.8	112.7	129	20	7/67	184.6	−5.6	181.9	−22.3	41.8	9.4	74.7	285.6	7.2
Xialiushi Formation														
hh31	26.8	112.7	201	4	5/8	196.6	−34.8	193.8	−34.5	36.8	12.8	75.1	231.5	11.1
hh32[b]	26.8	112.7	201	4	6/8	194.3	−23.5	192.5	−23.2	7.8	25.5	71.2	251.7	19.8
hh49	26.7	112.7	82	11	6/7	170	−11.1	170	−22.1	30.5	12.3	72.1	326.4	9.5
hh50	26.7	112.7	200	8	7/7	188.6	−30	184.2	−28.4	46.2	9	77.8	273.2	7.3
hh51	26.7	112.7	150	8	7/7	171.4	−42	164.3	−44.8	19.9	13.9	76	250	13.9
hh52[b]	26.7	112.7	73	4	4/4	185.8	−28.1	186.8	−31.7	28.2	17.6	78.6	257.9	14.8
hh53	26.7	112.7	102	15	7/7	172.1	−17.2	170	−31.5	31.3	13.9	76.6	338.5	11.7
hh56[b]	26.9	112.7	260	16	4/6	188.2	−40	184.8	−24.8	10.2	30.3	75.5	273.7	23.8
hh57	26.9	112.7	236	15	5/6	187.1	−53.2	176.9	−41.4	31.7	13.8	85.8	335.4	13.1
Mean					22	358.4	35.4	-	-	24.8	6.2	-	-	-
								358.9	35.4	37.0	5.0	82.6	300.7	4.4

[a]Same symbols as in Table 1.
[b]The data with $\alpha_{95} > 16°$ were not used to calculate the mean direction.

directions are horizontal and relatively dispersed in the NW direction, the mean direction of $\kappa 1$ axis after tilt correction is D = 319.6°, I = 0.5° and D = 319.7°, I = 0.3° for the Late Cretaceous and Paleogene red beds, respectively. The mean direction of $\kappa 3$ after tilt correction is oriented perpendicularly to bedding (I = 88.1° for the Late Cretaceous and I = 87.5° for the Paleogene). A mean anisotropy degree (P) of 1.13 (range of 1.02 to 1.32) is revealed for the Late Cretaceous red beds. Anisotropy shape factor (*T*) shows a dominance of oblate forms, with some prolate forms for samples with lower anisotropy (Figure 8b). For the majority of samples, the anisotropy degree (P) is quite low (average P value of 1.072), with the exception of three samples from the Paleogene red beds that have P values between 1.12 and 1.19 (Figure 8d). The AMS results indicate the presence of both strong and weak magnetic anisotropy in the red beds. In some samples, the values of P may exceed 1.2 and 1.1 for the Late Cretaceous and the Paleogene red beds, respectively. The AMS values in these samples are high for sedimentary rocks. The shape of the ellipsoids may vary between samples from different sites (Figures 8b and 8d). However, there is only a weak correlation (r = 0.21) between the shape of the AMS ellipsoid and the mean magnetic susceptibility (Figure 8e). There is no clear relationship (r = 0.08) between the observed inclination and the AMS parameters (P), as shown in Figure 8f.

[15] In addition, the mean $\kappa 1$ directions (about NW 320°) are significantly different from those (NE-SW) of the faults and the fold axis for the Cretaceous to Tertiary formations in the studied region (Figure 2). Furthermore, it appears unlikely that tectonic stress might have affected the AMS in part sediments rather than all sediments in the studied region. These features suggest that the AMS fabric with high anisotropy degree (P) in the red beds may be not directly related to the tectonic strain observed in the studied region. Alternatively, the high anisotropy degree (P) in some samples is probably due to the contribution of diamagnetic minerals such as calcite. Since calcite can be present as cement in red beds, it can have a strong preferred orientation [*Tan et al.*, 2003]. In this case, the composite AMS will have a greater anisotropy, which could explain the extreme high anisotropy degree (P) in some samples from the Hengyang basin. If the higher P values are produced by calcite, this suggests that high P values will not cause any deflection of the remanence direction. However, future investigations are required to determine the validity of this explanation. Given that the majority of samples have an AMS fabric with a near-vertical clustering of $\kappa 3$ axis together with $\kappa 2$ and $\kappa 1$ axes that lay in the bedding plane, this suggests that the red beds have not experienced significant strain due to compaction or tectonic stress.

4.2. Anisotropy of Isothermal Remanence

[16] Nineteen samples of the Late Cretaceous and 21 samples of the Paleogene were chosen from different sampling sites to perform the remanence anisotropy test for inclination shallowing [*Hodych and Buchan*, 1994].

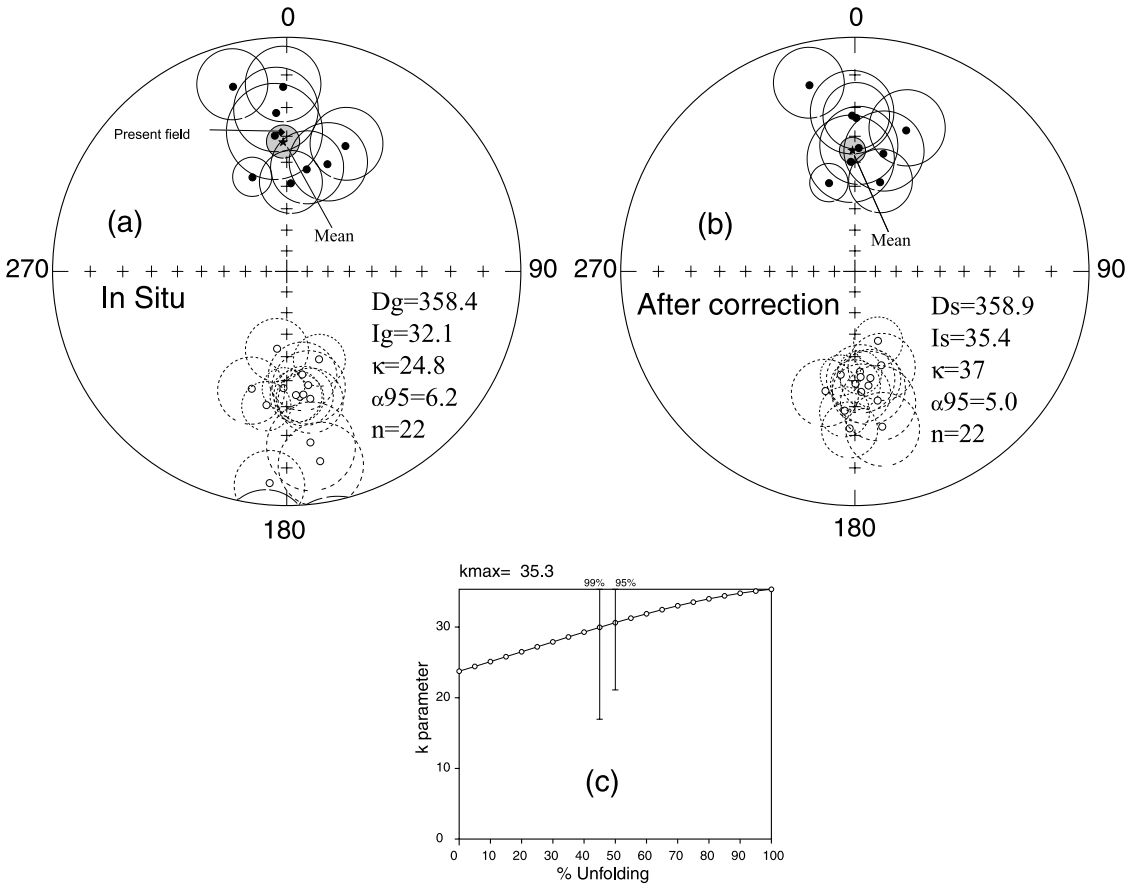

Figure 7. Equal-area stereographic projection of high-temperature component from Paleogene formation in (a) geographic and (b) stratigraphic coordinates, respectively. Lower (upper) hemisphere directions are marked with solid (open) symbols. (c) Progressive unfolding of the mean direction showing a maximum concentration at 100% unfolding.

For each of these representative block samples, a cylindrical specimen (2.2 cm length, 2.5 cm diameter) was drilled with its axis at 90° (±5°) to the bedding direction as described by *Hodych and Buchan* [1994].

[17] In magnetite-bearing sediments, inclination shallowing can be corrected using the anisotropy of magnetic susceptibility (AMS) or anisotropy of anhysteretic remanence (AAR) [*Bijaksana and Hodych*, 1997], but in hematite-bearing sediments, it is difficult to apply a large enough alternating field for the AAR to have a coercivity similar to that of the natural remanence. Hence another anisotropy test was performed by measuring an IRM parallel (IRMx) and perpendicular (IRMz) to the bedding plane to qualitatively evaluate the possibility of inclination shallowing [*Hodych and Buchan*, 1994]. The ratio of IRMz/IRMx can be related directly to the amount of inclination shallowing by tan $I_{obs}/\tan I_F = IRM_Z/IRM_X$ (I_{obs}, the inclination of remanence; I_F, the inclination of field in which it was acquired). For the majority of the Late Cretaceous (Figures 9a–9f) and Paleogene samples (Figures 9g–9l), the value of IRM_Z is the same as that of IRM_X when the applied field is below 200 mT, and the value of IRM_Z is slightly lower than that of IRM_X when the applied field is between 200 and 800 mT (Figure 9 and Table 3). The mean IRM_Z/IRM_X acquired between 200 and 800 mT is 0.8812 and 0.8801 for the Late Cretaceous and Paleogene rocks, respectively. At the same time, comparison of the thermal decay curves for IRM and NRM shows that hematite is the main contribute to NRM and IRM. Hence a better measure of the influence of anisotropy on the hematite remanence is obtained by using the high unblocking temperature data from thermal demagnetization of IRM (600°, 620°, 640°, 660°, 680°C) rather than to use the total IRM acquired between 200 and 800 mT. Magnetic mineral transformations were monitored during thermal demagnetization by measuring bulk susceptibility after each heating step of the IRM, using a Bartington susceptibility meter. The relative constancy of the susceptibility indicated that no chemical change of the magnetic minerals in the red beds has taken place during heating (Figure 9m). This suggests that the value of IRM_Z/IRM_X after heating is reliable. The mean IRM_Z/IRM_X obtained from all sites of thermal demagnetizaion between 600°C and 680°C is 0.8828 for the Late Cretaceous and 0.8604 for the Paleogene, close to the mean IRM_Z/IRM_X of 0.8812 for the Late Cretaceous and 0.8801 for the Paleogene via IRM acquired between 200 and 800 mT. Therefore it should make little difference which of these two estimates of IRM_Z/IRM_X are used to calculated inclination shallowing (Table 3). Substituting the ratios for $\tan (I_{obs}/\tan I_F) = IRM_Z/IRM_X$, the corrected inclination is 33.1° (I_{obs} = 29.9°) for the Late Cretaceous, and 39.6° (I_{obs} = 35.4°) for the Paleogene red beds. Hence

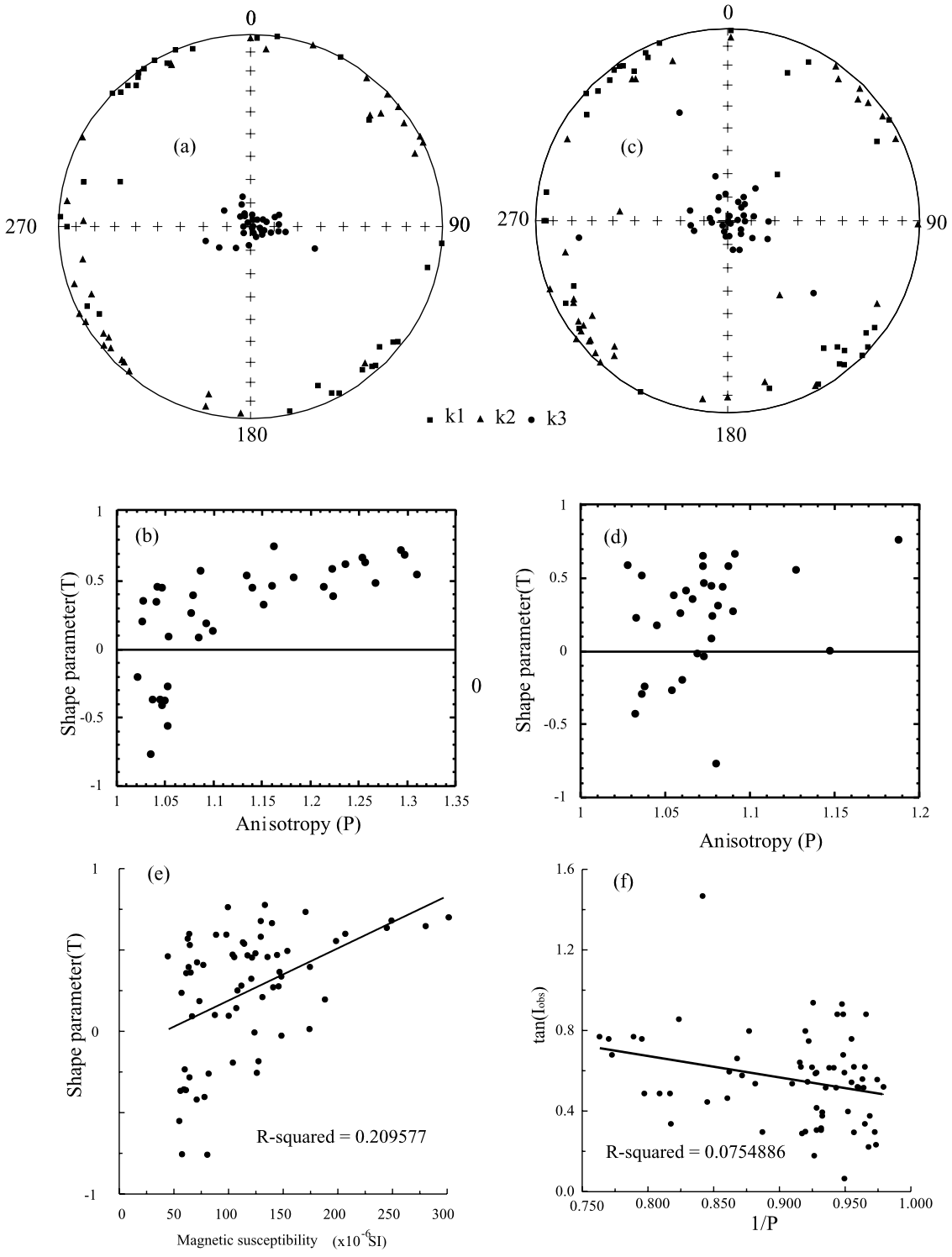

Figure 8. (a and c) Stereonet projection of AMS in stratigraphic coordinates for Late Cretaceous and Paleogene formations, respectively, for κ1, maximum; κ2, intermediate; κ3, minimum. (b and d) Plots of shape parameter (*T*) versus anisotropy degree (P) for Late Cretaceous and Paleogene formations, respectively. (e) Plot of shape parameter (*T*) versus magnetic susceptibility for all the Late Cretaceous and Paleogene samples. There is no distinct relation between magnetic susceptibilities and the shape of the AMS ellipsoids. (f) Correlation between the observed tan(I_{obs}) and the AMS parameters (P = κ1/κ3). The much lower correlation coefficient (R) shows that the observed inclination is independent of the AMS parameters.

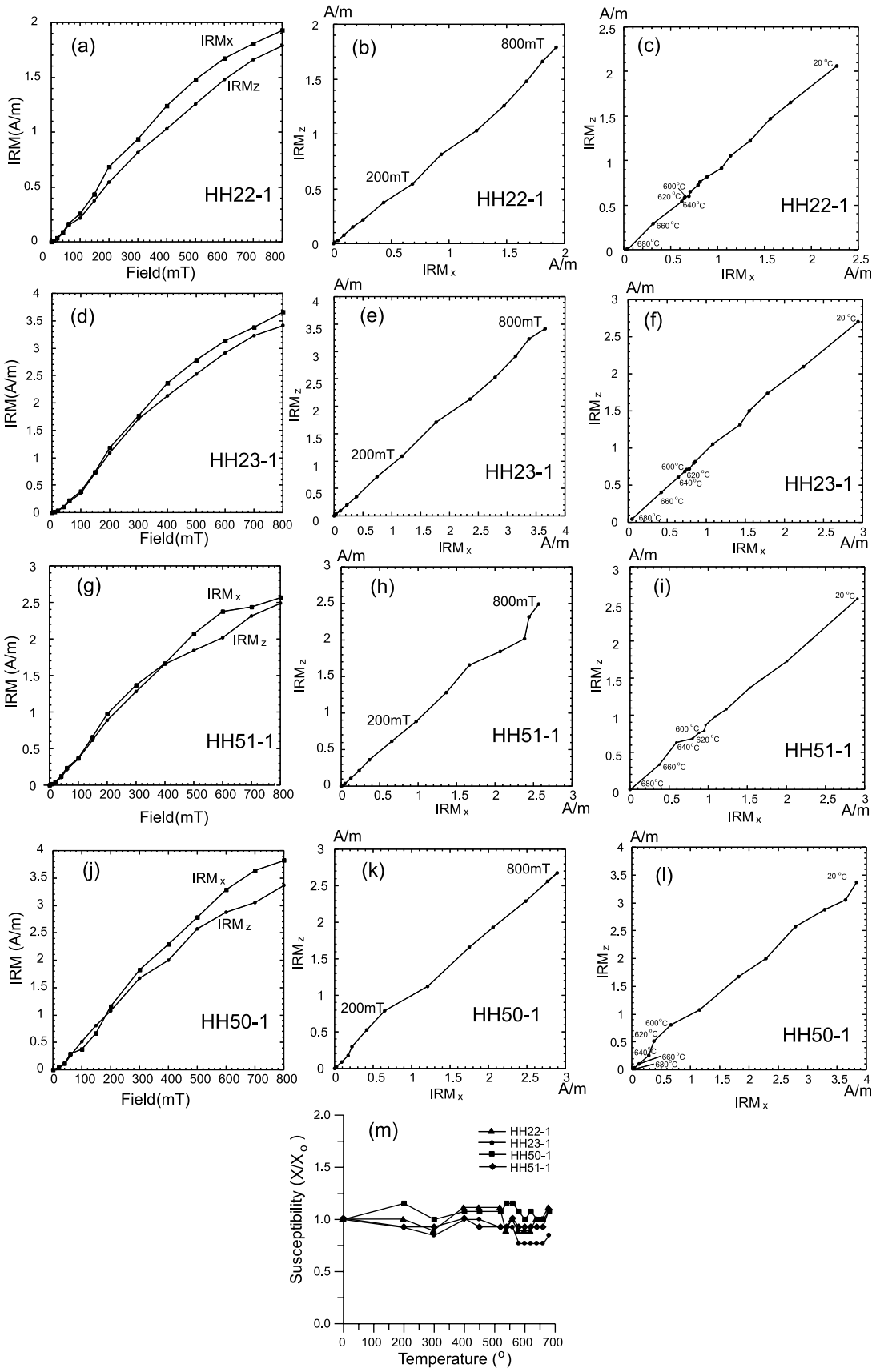
(a)
IRMx
IRMz
IRM(A/m)
Field(mT)
HH22-1
(b)
800mT
200mT
IRM z
IRM x
A/m
HH22-1
(c)
20 °C
600°C
620 °C
640°C
660 °C
680°C
IRM z
IRM x
A/m
HH22-1
(d)
IRM(A/m)
Field(mT)
HH23-1
(e)
800mT
200mT
IRM z
IRM x
A/m
HH23-1
(f)
20 °C
600°C
620 °C
640°C
660 °C
680°C
IRM z
IRM x
A/m
HH23-1
(g)
IRM x
IRM z
IRM (A/m)
Field(mT)
HH51-1
(h)
800mT
200mT
IRM z
IRM x
A/m
HH51-1
(i)
20 °C
600 °C
620 °C
640°C
660 °C
680°C
IRM z
IRM x
A/m
HH51-1
(j)
IRM x
IRM z
IRM (A/m)
Field(mT)
HH50-1
(k)
800mT
200mT
IRM z
IRM x
A/m
HH50-1
(l)
20 °C
600°C
620 °C
640°C
660 °C
680°C
IRM z
IRM x
A/m
HH50-1
(m)
HH22-1
HH23-1
HH50-1
HH51-1
Susceptibility (X/X o)
Temperature (°)

Figure 9

Table 3. Anisotropy of Isothermal Remanence Magnetization for Late Cretaceous and Paleogene Red Beds From the Hengyang Basin[a]

Site	I_{obs}	IRM_Z/IRM_x Acquired Between 200 and 800 mT	IRM_Z/IRM_x Acquired Above 600°C
Late Cretaceous Formation			
hh1	26.1	0.917	0.796
hh2a	32.1	0.807	0.906
hh2b	32.1	0.899	0.868
hh2c	32.1	0.892	0.895
hh3a	32.5	0.844	0.852
hh3b	32.5	0.954	0.948
hh5a	13.1	0.891	0.848
hh5b	13.1	0.832	0.841
hh6	33	0.737	0.774
hh7	34.1	0.876	0.955
hh22	39.9	0.941	0.903
hh23	41	0.814	0.872
hh37	27.8	0.984	0.876
hh35	27.4	0.913	0.815
hh36	26.7	0.908	0.897
hh38	38.5	0.923	0.931
hh42	21.5	0.856	0.812
hh41	25	0.873	0.922
Mean		0.8812	0.8828
Paleogene Formation			
hh9	43.6	0.838	0.801
hh10	23.5	0.906	0.79
hh14	38.7	0.829	0.887
hh15	11.4	0.894	0.838
hh17	47.1	0.771	0.772
hh18	46.8	0.936	0.792
hh54	22.3	0.941	0.93
hh56	24.8	0.818	0.813
hh53	31.5	0.793	0.819
hh52	31.7	0.879	0.846
hh51	44.8	0.922	0.877
hh50a	28.4	0.83	0.825
hh50b	28.4	0.871	0.979
hh49	22.1	0.927	0.968
hh48a	34.4	0.976	0.774
hh48b	34.4	0.865	0.886
hh47a	24.7	0.856	0.843
hh47b	24.7	0.936	0.945
hh46	35.3	0.966	0.95
hh42	21.5	0.856	0.812
hh41	25	0.873	0.922
Mean		0.8801	0.8604

[a] I_{obs}, mean inclination of site; IRM_Z/IRM_x, isothermal remanence measured perpendicular to bedding/isothermal remanence measured parallel to bedding for IRM acquired between 200 and 800 mT.

the red beds have, on average, undergone about 3° and 4° of inclination shallowing for the Late Cretaceous and the Paleogene, respectively, causing less than 2° of paleolatitude underestimation. However, there is distinct difference between the results of the two AIR methods in some sites (for example, hh18 and hh48a), indicating that the performance of the paleomagnetic inclination correction varies between sites. Furthermore, there appears to be no significant correlation between tan (I_{obs}) and the ratios of IRM_Z/IRM_X (Figure 10). The correlation coefficients (R) are only 0.149 and 0.0823 for the Late Cretaceous and Paleogene red beds, respectively, which imply that the observed inclinations have suffered little from the effect of depositional compaction. The result suggests that sediment compaction has not caused significant inclination shallowing at 95% confidence limits in the Late Cretaceous and Paleogene rocks of the Hengyang basin. Nevertheless, we note that the investigated samples cover a large time interval and the inclination values vary in a large range (Table 3). This suggests that a lack of correlation between tan (Iobs) and AIR (Figure 10) cannot be used as evidence for a lack of inclination shallowing. Thus, as discussed above, we considered that depositional compaction caused up to 3–4° of inclination shallowing for the Late Cretaceous and the Paleogene red beds.

5. Discussion

5.1. Comparison With Other Late Cretaceous and Paleogene Paleomagnetic Result From the SCB

[18] A large number of paleomagnetic results have been derived from Late Cretaceous and Paleogene rocks from the SCB (Table 4). Obviously, the poles are quite scattered because most of the Late Cretaceous poles came from the strongly faulted cratonic margin in the SCB (Figure 11a). One group of poles was obtained from the coastal provinces of Fujian, Guangdong and Zhejiang, located between the Zhenhe-Dapu and Changle-Nanou faults; a second group of poles was obtained from the western part of Sichuan province, situated to the east of Longmenshan fault zone, or from the Chuan-Dian fragment located between the Red River faults zones and the Xianshuihe-Xiaojiang fault zones (Figure 1). Some poles have clearly suffered from local rotations about vertical axes, as suggested by the original authors [*Enkin et al.*, 1991; *Gilder et al.*, 1993, 1999; *Otofuji et al.*, 1998]. For example, the coastal provinces of Fujian and Guangdong are rotated clockwise with respect to the stable SCB (Figure 11a) [*Gilder et al.*, 1993]. The western parts of Sichuan province show local counterclockwise rotations with respect to the stable SCB [*Enkin et al.*, 1991; *Huang and Opdyke*, 1992]. This streaking of Late Cretaceous poles from the SCB discourages us from using the average of currently available poles as a reference for the entire SCB. It is apparent in Figure 11a that the Late Cretaceous pole from the Nanjing area [*Kent et al.*, 1986] and from Hong Kong [*Chan*, 1991] lie far away from those for the stable SCB. The Late Cretaceous poles

Figure 9. (a, d and g, j) Application of an IRM at 45° to the bedding which produces an isothermal remanent magnetization whose components IRMx (parallel to bedding) and IRMz (perpendicular to bedding) are plotted as function of increasing field (Late Cretaceous (Figures 9a and 9d); Paleogene (Figures 9g and 9j)). (b, e and h, k) Gradient of the best fit correlation line of IRMz versus IRMx, between 200 and 800 mT (hematite component), which provides the IRMz/IRMx ratio that is used to estimate inclination shallowing in the sediments. (c, f and i, l) Slope of the thermal demagnetization of IRMx and IRMz, between 600° and 680°, which provides a measure of the magnetic anisotropy of high blocking temperature hematite [*Hodych and Buchan*, 1994] (m). Mass susceptibility versus temperature curves used to monitor chemical changes induced during the thermal demagnetization of IRM.

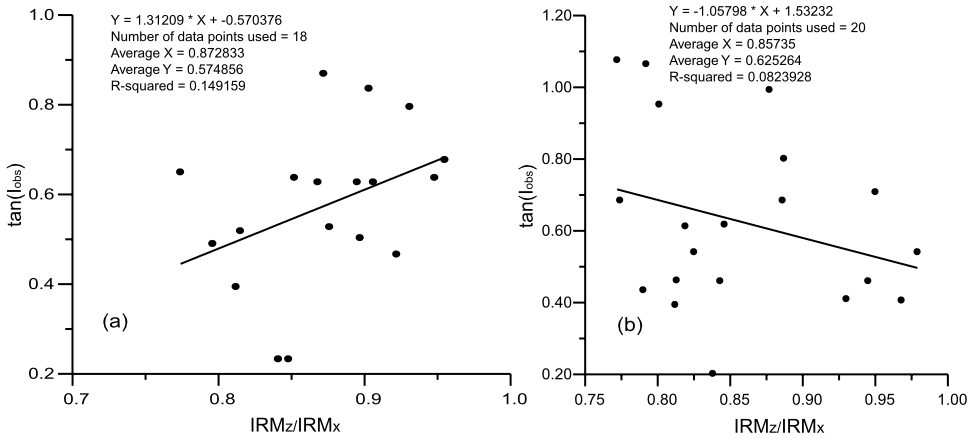

Figure 10. Correlation between the observed $\tan I_{obs}$ and IRM_z/IRM_x is shown (a) for the Late Cretaceous red beds and (b) for the Paleogene red beds. The correlation line's estimate of $\tan I_{obs}$ when $IRM_z/IRM_x = 1$ predicts tan I_H corrected for inclination shallowing. The low correlation coefficient (R) shows that the observed inclinations have likely not suffered from the significant effect of depositional compaction for the Late Cretaceous and Paleogene red beds in the Hengyang basin. The correlation coefficient (R) for the Late Cretaceous red beds (Figure 10a) is a little higher than that for the Paleogene red beds (Figure 10b).

from the Nanjing area [*Kent et al.*, 1986] may have been acquired during the northward motion of the region during the Paleogene [*Enkin et al.*, 1991]. The Late Cretaceous pole from Hong Kong was reconsidered as Early Cretaceous or Late Jurassic age which is confirmed by the high-precision radiometric age between 165 and 140 Ma [*Sewell et al.*, 1998]. However, the Late Cretaceous poles from the Hengyang basin (Hunan province), Guanying area (Sichuan

Table 4. Late Cretaceous and Paleogene Poles From South China[a]

Area	Slat	Slon	N(n)	Plat	Plon	A_{95}	Reference
				Paleogene			
Guangxi	22.7	108.3	5(31)	83.8	236	4.3	*Zhao et al.* [1994]
Guangxi	23.5	107.2	1(17)	58.6	18.2	7.4	*Gilder et al.* [1993]
Sichuan	30	13	7(97)	76.8	299.9	3.5	*Enkin et al.* [1991]
Sichuan	26.5	102.3	7(36)	70.6	286.1	11.6	*Huang and Opdyke* [1992]
Hunan	26.9	112.6	22(145)	82.6	300.7	4.4	this study
Yunnan	25.8	101.5	9	64	211.2	4.3	*Yang et al.* [2001]
Yunnan	26.1	101.7	16	70.1	224.6	4.9	*Yoshioka et al.* [2003]
Yunnan	25.7	101.3	10	72.3	218.4	4.5	*Yoshioka et al.* [2003]
				Late Cretaceous			
Nanjing	32	119	10(43)	76.3	172.6	10.3	*Kent et al.* [1986]
Hunan	26.9	112.6	26(182)	71.9	236.3	4.7	this study
Anhui	30.8	118.2	7	82.4	221.5	6.7	*Gilder et al.* [1999]
Yunnan	25.9	101.7	21	64.6	199.6	3.2	*Otofuji et al.* [1998]
Sichuan	30	103	11(87)	78.3	274.5	4.2	*Enkin et al.* [1991]
Sichuan	29.1	104.6	9	68	231.6	8.1	*Enkin et al.* [1991]
Sichuan	26.5	102.4	18(91)	81.5	220.9	7.1	*Huang and Opdyke* [1992]
Fujian	26	117.2	5	66.9	221.4	5.4	*Zhai et al.* [1992]
Fujian	26	117.3	1(20)	65.1	207.2	5	*Gilder et al.* [1993]
Guangdong	23.1	113.3	1(19)	56.2	211.5	3.9	*Gilder et al.* [1993]
Guangdong	24.3	114.8	1(43)	66	221.5	3.4	*Hsu* [1987]
Hongkong	22.2	114.2	12	78.2	171.9	8.7	*Chan* [1991]
				Early Cretaceous			
Sichuan	27.9	102.3	-	84.8	245.8	5.7	*Tamai et al.* [1996]
Sichuan	30.4	103.8	4(35)	67.7	214.3	13.6	*Enkin et al.* [1991]
Sichuan	30.0	103.0	6	73.1	248.3	10.3	*Enkin et al.* [1991]
Sichuan	26.8	102.5	7	69	204.6	4.3	*Huang and Opdyke* [1992]
Guangxi	22.7	108.7	8	86.5	26.4	6.8	*Gilder et al.* [1993]
Hainan	18.8	109.1	17	77.1	162.1	4.4	*Liu and Morinaga* [1999] and *Li et al.* [1995]
Zhejiang	29.7	120.3	-	77.1	227.6	5.5	*Lin et al.* [1985]
Yunnan[b]	25.0	101.5	11	49.5	189.3	15.2	*Funahara et al.* [1992]
Mean			8	78.7	215.7	8.2	this study

[a]Slat (Plat), latitude of site (pole); Slon (Plon), longitude of site (pole); N/n, number of sites(samples); A_{95}, the radius that the mean pole lies within 95% confidence.
[b]Pole suspected suffering local rotation.

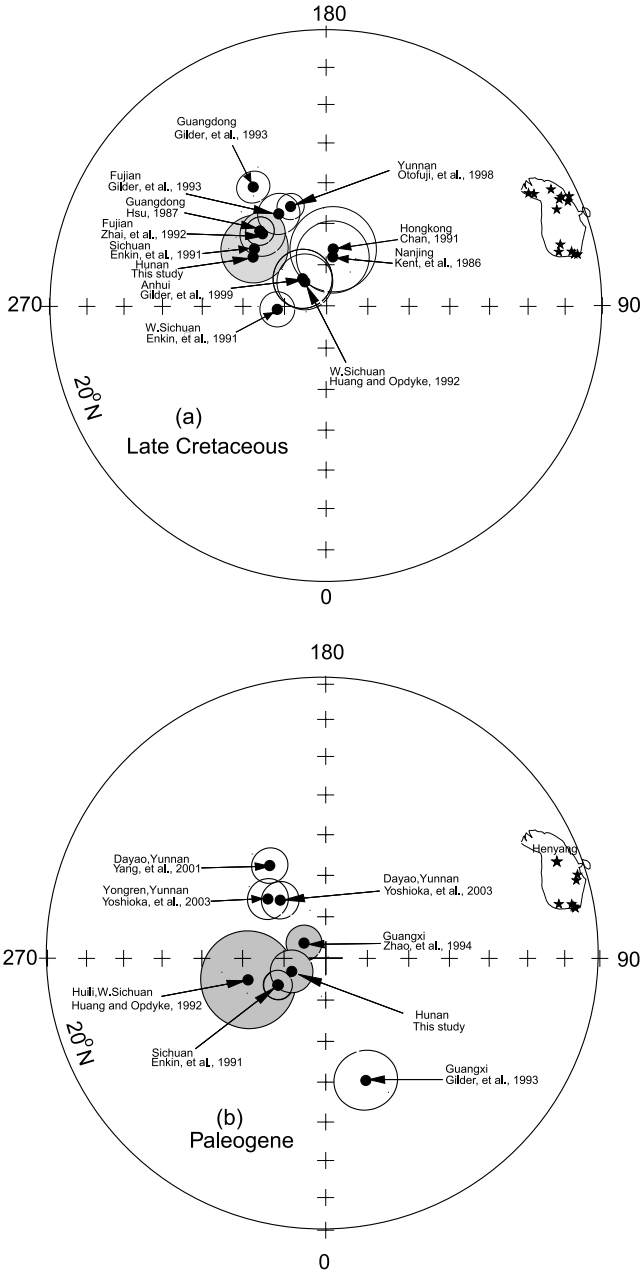

Figure 11. Equal-area projections of (a) Late Cretaceous and (b) Paleogene paleopoles from this study (stars) and published studies (solid circles) for the entire SCB. Poles with shaded confidence circles are from assumed stable zones, with the remainder from zones that are thought to have undergone local tectonic rotation.

province) [*Enkin et al.*, 1991], Fujian province [*Zhai et al.*, 1992], and Guangdong province [*Hsu*, 1987] are overlapped at the 95% confidence level. The observations indicate no relative movement from the eastern part to the western part of the SCB, which implies that a large part of the SCB has behaved as a coherent block since the Late Cretaceous, as suggested by *Yang and Besse* [2001] and *Morinaga and Liu* [2004].

[19] The available Paleogene poles from the Chuan-Dian fragment located between the Red River Fault and Xianshuihe-Xiaojiang fault zones, and the stable areas of the SCB are distributed along a small circle centered on the sampling areas (Figure11b), which implies that insignificant latitudinal motion has occurred between the sampling sites in these areas within paleomagnetic uncertainties. The Chun-Dian fragment area experienced a clockwise rotation relative to the stable SCB since the Paleogene [*Yang et al.*, 2001; *Yoshioka et al.*, 2003]. The Youjiang area of Guangxi province has also suffered from a local counterclockwise rotation relative to the stable SCB due to a left-lateral strike slip of the Youjiang fault [*Gilder et al.*, 1993], while insignificant rotation was observed in the Nanning area of Guangxi province by *Zhao et al.* [1994]. The Paleogene pole from the Hengyang basin is not distinguishable from those of Sichuan [*Huang and Opdyke*, 1992; *Enkin et al.*, 1991] and Guangxi [*Zhao et al.*, 1994] at the 95% confidence level (Figure 11b), which further confirm that these regions between the Longquanshan (Sichuan) and the southeast Coast province can be regarded as a single stable block since the Late Cretaceous. Thus the Late Cretaceous and Paleogene poles from the Hengyang basin can be regarded as the reference poles of the stable SCB.

[20] Comparing the observed paleomagnetic direction between the Late Cretaceous (D = 15.6°, I = 29.9°, α_{95} = 4.7°) and the Paleogene (D = 358.9°, I = 35.4°, α_{95} = 5.0), these results show a clockwise rotation of 16.7 ± 5.0° without significant latitudinal motion. This clockwise rotation of the SCB may be related to the eastward movement of the main body of Tibetan Plateau and south China produced by the collision of India and Asia in the west, and the subduction of circum-Pacific to eastern Asia, which have occurred since the Cenozoic.

5.2. Comparison With the Late Cretaceous and Paleogene Poles From Other Blocks in Asia

[21] Using the 80–50 Ma mean pole (K2) of the Eurasian APWP, proposed by *Besse and Courtillot* [2002], the expected Late Cretaceous declination and paleolatitude for the sampling area are 10.4 ± 3.9° and 27.0 ± 3.9°N, respectively (reference site 26.9°N, 112.6°E). Comparing the reference direction deduced from Eurasian APWP with observed from the Hengyang basin, the declination and latitudinal differences of the sampling area of SCB are 5.2 ± 4.8° and 11.0 ± 4.5°, and −9.4 ± 4.5° and 12.8 ± 4.0° for the Cretaceous and Paleogene, respectively (Table 5). These results could imply a large intracontinental crustal shortening (more than 1100Km within the uncertainty) between the SCB and Eurasia (or Siberia) since the Paleogene. This case is similar to the anomalously shallow inclinations reported from central Asia since the Cretaceous by many authors [*Halim et al.*, 1998; *Gilder et al.*, 2001; *Tan et al.*, 2003]. Several hypotheses were proposed to explain this inclinational discrepancy such as poor age control, synsedimentary or compaction-induced inclination shallowing, nondipolar geomagnetic field geometry, tectonic shortening, or a poorly constrained APWP for Eurasia and or nonrigidity of the Eurasian plate [*Gilder et al.*, 2001; *Tan et al.*, 2003; *Chauvin et al.*, 1996; *Halim et al.*, 1998; *Li et al.*, 1988; *Chen et al.*, 1992; *Cogné et al.*, 1999]. However, no striking anomaly of the geomagnetic field was present during the Cenozoic and Mesozoic period [*Besse and Courtillot*, 1991; *Kent and Smethrust*, 1998]. Many studies have identified

Table 5. Late Cretaceous and Paleogene Paleopoles for the Chinese and Adjacent Blocks[a]

						Relative to SCB		Relative to Eurasia		
Block	Age	Lith	Plat	Plon	A_{95}	Latitudinal Difference	Rotation	Latitudinal Difference	Rotation	Reference
Tarim	E3-N1	Sed	71.2	226.7	6.7	−1.5 ± 5.9	19.1 ± 6.2	14.2 ± 5.5	9.8 ± 5.9	*Chen et al.* [1992]
Tarim	E1	Sed	58.1	202	12.7	3.4 ± 9.9	36.1 ± 10.4	9.4 ± 9.6	26.7 ± 10.5	*Gilder et al.* [1996]
Qaidam	E	Sed	63.4	211.2	9.9	−0.6 ± 8.0	29.2 ± 8.4	12.2 ± 7.7	19.9 ± 8.3	*Chen et al.* [2002]
Junggar	E1-2	Sed	74.3	223.1	6.4	−1.0 ± 5.7	16.8 ± 6.0	11.8 ± 5.3	7.4 ± 5.8	*Chen et al.* [1991]
Kyrgyzstan	E	Bas	75	220.9	7.5	−1.8 ± 6.4	16.4 ± 6.7	11.0 ± 6.0	7.0 ± 6.6	*Thomas et al.* [1993]
Tianshan	E	Bas	77	187.5	4.4	−10.0 ± 4.6	15.6 ± 4.8	2.8 ± 4.0	6.2 ± 4.7	*Bazhenov et al.* [2002]
SCB	E	Sed	82.6	300.7	4.4	-	-	12.8 ± 4.0	−9.4 ± 4.5	this study
NCB	E	Bas	85.5	196.4	8.7	−7.7 ± 7.7	6.1 ± 7.5	5.0 ± 6.8	3.2 ± 7.7	*Zheng et al.* [2002]
Mongolia	E	Bas	84	288.8	4.5	−1.3 ± 4.6	1.5 ± 4.9	11.4 ± 4.1	−7.2 ± 4.6	*Hankard et al.* [2003]
NCB	K2	Bas	79.4	191.3	6.3	−12.4 ± 5.8	−3.8 ± 6.4	−1.5 ± 5.4	1.4 ± 6.2	*Zheng et al.* [2002]
Mongolia	K2	Bas	73.9	244.7	8.3	0.4 ± 7.0	−3.3 ± 7.3	11.4 ± 6.7	1.9 ± 7.1	*Hankard et al.* [2003]
Liaodong	K2	Sed	59.4	205.5	7.3	−5.5 ± 6.4	17.5 ± 6.8	5.5 ± 6.1	22.7 ± 6.6	*Lin et al.* [2003]
SCB	K2	Sed	71.9	236.3	4.7	-	-	11.0 ± 4.5	5.2 ± 4.8	this study
Siberia	K2	Bas	78.3	271	9.9	0.1 ± 8.0	−11.1 ± 8.4	11.0 ± 7.8	−6.0 ± 8.2	*Bragin et al.* [1999]
Tarim	K1	Sed	67.0	214.1	6.0	3.5 ± 7.5	12.1 ± 8.1	8.0 ± 4.8	11.8 ± 5.2	*Chen et al.* [2002]
Qilianshan	K1	Sed	62.2	193.4	3.2	−4.0 ± 6.5	19.3 ± 7.1	0.5 ± 3.1	19.1 ± 3.5	*Yang et al.* [2001]
NCB	K1	Sed	75.8	208.7	7.5	−0.7 ± 8.2	3.5 ± 8.9	3.7 ± 5.9	3.2 ± 6.5	*Ma et al.* [1993]
SCB	K1	Sed	78.7	215.7	8.2	-	-	4.4 ± 6.3	0.3 ± 7.0	this study
Eurasia	E (50–30 Ma)		81	163.5	3.3					*Besse and Courtillot* [2002]
Eurasia	K2 (80–50 Ma)		80.7	199.6	3.9					*Besse and Courtillot* [2002]
Eurasia	K1(140–80 Ma)		79.0	192.6	2.7					*Besse and Courtillot* [2002]

[a]Lith, lithology; Bas, basalt; Sed, sediments (red bed)); Plat (Plon), latitude (longitude) of pole; A_{95}, the radius that the mean pole lies within 95% confidence. Rotation and latitudinal differences are evaluated by comparison between the observed paleomagnetic result and that expected from the stable SCB and Eurasia (reference point is 26.9°N, 112.6°E). Plus/minus, southward/northward or counterclockwise (clockwise rotation).

that the SCB and NCB were fully assembled with Eurasia by Early Cretaceous [*Yang et al.*, 1992; *Gilder and Courtillot*, 1996], requiring that all ocean basins between plates such as the NCB, SCB, Mongolia and Siberia should have been closed prior to that time. It is clear that there is a lack of geological evidence to account for more than 1100 km of shortening in the north of the SCB or Mongolia. Although 10% (3–4°) of inclination shallowing (less than 2° of paleolatitude) of these red beds could be related to synsedimentary or postdepositional compaction that was identified by the analysis of AIR in the Hengyang basin, the inclination differences between the observed and deduced are still too large during the Cretaceous and Paleogene. Hence the inclination difference between the SCB and Eurasia during the Late Cretaceous and Paleogene cannot be resulted only from inclination shallowing. The age of Late Cretaceous and Paleogene red beds in the Hengyang basin are also well constrained by fossils, Ar-Ar dating and magnetostratigraphic data. Hence we suggest that the Late Cretaceous and Paleogene remanences are primary without significant inclination shallowing. On the basis of the new Late Cretaceous and Paleogene paleomagnetic results, we can discuss further tectonic evolution of the SCB with respect to other blocks of the Asian blocks since the Late Cretaceous.

[22] The representative Cretaceous and Paleogene poles from the main Chinese blocks (NCB, SCB, Tarim, Qaidam, Liaodong), including adjacent blocks, Siberia (SIB), Mongolia, Junggar, Tianshan, Kyrgyzstan, and Eurasia, are listed in Table 5. As shown in Figure 12, the Early Cretaceous poles from the SCB, NCB, and Eurasian block are indistinguishable at the 95% confidence level (Figure 12a), and the Late Cretaceous poles from the SCB, Mongolia [*Hankard et al.*, 2003] and Siberia [*Bragin et al.*, 1999] are statistically indistinguishable from each other with overlapped confidence circles (Figure 12b). The Paleogene poles for the SCB are also indistinguishable from that of Mongolia [*Hankard et al.*, 2003] (Figure 12c and Table 5). These results support the interpretation that the NCB, SCB, Siberia and Mongolia were sutured prior to the late Jurassic [*Yang et al.*, 1992; *Gilder and Courtillot*, 1997; *Halim et al.*, 1998]. In the other words, the SCB has experienced neither significant rotation nor latitudinal translation relative to Siberia and Mongolia since the Late Cretaceous. However, if the synthesis poles of Eurasia were used [*Besse and Courtillot*, 2002], then the SCB, Mongolia and Liaodong areas might experienced a significant northward latitudinal motion relative to the Eurasia since the Late Cretaceous.

[23] We also note the insignificant discordance of the Paleogene poles between central Asia and eastern Asia (SCB, Siberia and Mongolia) (Figure 12c). A large number of Paleogene poles from central Asia were obtained from the areas of Tianshan, Qaidam [*Chen et al.*, 2002], Tarim [*Chen et al.*, 1992; *Gilder et al.*, 1996], Junggar [*Chen et al.*, 1991], and Kyrgyzstan blocks [*Thomas et al.*, 1993], which are far sided with respect to the Eurasian APWP [*Besse and Courtillot*, 2002] (Figure12b). We compared the Paleogene poles from central Asian blocks (Tarim, Qaidam, Junggar, Tianshan, Kyrgyastan) with coeval reference poles from the SCB and Eurasia (Table 5). We note that there is a significant latitudinal difference (more than 10°) of Tertiary poles (50–30 Ma) for Eurasian and Tianshan. However, we also note that central Asia blocks have not experienced any significant northward motion within paleomagnetic uncertainties relative to the stable SCB since the Paleogene, although a distinct relative clockwise rotation has occurred (Table 5).

[24] To test whether the red beds have suffered compaction-induced inclination shallowing, an increasing number of paleomagnetic studies have been carried out on Cretaceous-Paleogene volcanic rocks from Asia [*Thomas et al.*, 1993; *Halim et al.*, 1998; *Bragin et al.*, 1999; *Zheng et*

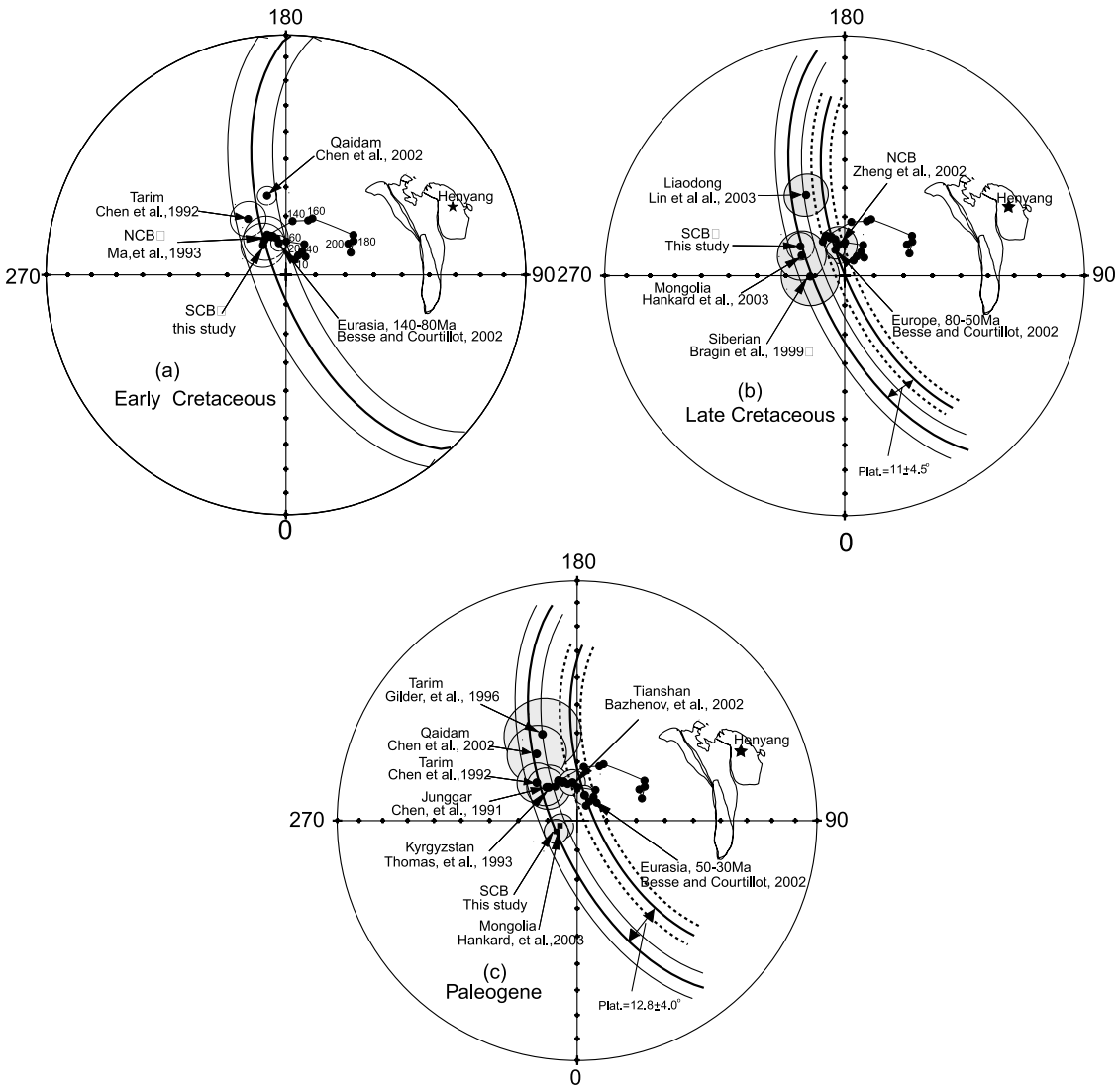

Figure 12. Equal-area projections of (a) the Early Cretaceous poles, (b) Late Cretaceous poles, and (c) Paleogene paleopoles for the Chinese blocks and adjacent blocks.

al., 2002; *Gilder et al.*, 2003; *Bazhenov et al.*, 2002; *Hankard et al.*, 2003]. However, since the studies used either an insufficient number of flows to average out geomagnetic secular variation, or lacked reliable dating and/or bedding control of the flow units, the poles obtained from these studies have also recently been debated [*Bazhenov et al.*, 2002; *Hankard et al.*, 2003; *Zheng et al.*, 2002]. For example, the results of the Paleogene flows from north of Tianshan show no significant inclination shallowing with respect to that calculated from the synthetic Eurasian APWP, even if the reported K-Ar age of the volcanics are ranged from 50 to 74 Ma [*Bazhenov et al.*, 2002]. The paleolatitudes of Early Cretaceous red beds are generally lower than that of volcanic rocks from the western Tarim Basin, although the difference is not significant at the 95% confidence limits [*Gilder et al.*, 2003]. The Late Cretaceous pole obtained from the basalt in Inner Mongolia, China [*Zheng et al.*, 2002], which fell close to the coeval pole for Eurasia, however, is suspected due to uncertainty of the bedding orientation control [*Zhao et al.*, 2004]. On the contrary, the paleomagnetic results of late Mesozoic and Cenozoic volcanic rocks from Mongolia [*Hankard et al.*, 2003], Siberia [*Bragin et al.*, 1999], and Kyrgyzstan [*Thomas et al.*, 1993], have inclination similar to those obtained from red beds, which are much shallower than those expected from the Eurasian APWP [*Besse and Courtillot*, 1991, 2002].

[25] The APWP for Eurasia [*Besse and Courtillot*, 1991, 2002] is usually employed as a reference curve for late Mesozoic-Cenozoic paleomagnetic studies in Asia. As we know, the Late Cretaceous and Paleogene reference poles for Eurasia are based mainly on data from northwestern Europe (e.g., Germany, United Kingdom, and France), with few from Siberia or eastern Asia, and on a compilation of worldwide selected poles related one to each other through oceanic kinematics and transferred onto the Eurasian plate. However, as pointed by *Cogné et al.* [1999], the large size of Eurasia covered more than 180° in longitude, such that a small rotation in declination in western Eurasia can translate into large latitudinal motion at the eastern margin of Eurasia and Siberia. On the other hand, recent geological and geophysical evidence suggests that the European

platform has not behaved as a single stable plate since the Late Cretaceous. First, the large-scale three-dimensional (3-D) gravity data shows that the European platform can be divided clearly into two parts: the East European Craton (EEP) and western Europe, which were separated by a transition area (Tornquist-Teisseyre zone) from the Proterozoic to the Cenozoic [*Yegorova and Starostenko*, 1999]. Second, deformation in Eurasia is very complex due to the continued collision between Africa and Eurasia during the Miocene, collision of the European plate with Apulia, the Alpine-Carpathian terranes, until 17 Ma, and subduction of the eastern Mediterranean Sea beneath the Eurasia margin since the Cenozoic [*Trifonov*, 2004]. These tectonic movements have controlled the evolution of European crust since the beginning of the Cenozoic [*Michona et al.*, 2003]. In this case, Eurasia may have not behaved as an entirely rigid plate since the Cenozoic, due to differences of continental shortening in the Alpine and Himalayan belt. Since there are few reliable Late Cretaceous and Paleogene poles for Siberia, which makes it difficult to discuss the tectonic history of central Asia relative to Siberia, we prefer to use the Late Cretaceous and Paleogene poles of the SCB as proxy poles for Siberia, rather than the transferred poles from Europe. It is therefore important to obtain late Mesozoic and early Cenozoic results from Siberia, to facilitate an improved understanding of the plate motions of Eurasia and the tectonic evolution of eastern Asia.

6. Conclusion

[26] We have presented new Late Cretaceous and Paleogene results from the Hengyang basin in the SCB. The characterization remanent magnetization (ChRM) direction from the Late Cretaceous and the Paleogene red beds pass reversal tests, while AIR measurement suggest that only 3°–4° of inclination shallowing has resulted from depositional compaction. Consequently, the Late Cretaceous and Paleogene results from the Hengyang basin can be considered to represent a primary remanence. These results indicate that between the Late Cretaceous and Paleogene, the SCB rotated 16.7 ± 5.0° with no significant latitudinal motion. On the basis of comparisons with the paleomagnetic results of Late Cretaceous and Paleogene basalts from Mongolia and Siberia, our results demonstrate a lack of significant relative north-south movement between the SCB and Siberia during this time interval. Furthermore, central Asia, including the Tarim, Qaidam, Junggar, Tianshan, and Kyrgyzstan blocks, has not experienced significant latitudinal motion relative to the stable SCB if new Late Cretaceous and Paleogene results are used. These findings are contrary to those obtained if the synthetic reference APWP of Eurasia is used.

[27] **Acknowledgments.** We particularly wish to acknowledge Patrick Taylor and two anonymous reviewers for very careful and constructive comments on an early version of the manuscript. We also thank Tim Rolph for valuable suggestions that significantly improved the manuscript. This study was funded by the Chinese National Natural Science Foundation (49925410) and partly by the Chinese NSF grants 40132020 and 40102021 and the Key Laboratory of Crust Deformation and Processes, CAGS. Paleomagnetic data were analyzed using R. Enkin's and J. P. Cogné's computer program package.

References

Bazhenov, M., L. Alexander, and V. Mikolaichuk (2002), Paleomagnetism of Paleogene basalts from the Tien Shan, Kyrgyzstan: Rigid Eurasia and dipole geomagnetic field, *Earth Planet. Sci. Lett.*, *195*, 155–166.

Besse, J., and V. Courtillot (1991), Revised and synthetic apparent polar wander paths of the African, Eurasian, North American and Indian plates, and true polar wander since 200 Ma, *J. Geophys. Res.*, *96*, 4029–4050.

Besse, J., and V. Courtillot (2002), Apparent and true polar wander and the geometry of the geomagnetic field over the last 200 Myr, *J. Geophys. Res.*, *107*(B11), 2300, doi:10.1029/2000JB000050.

Bijaksana, S., and J. P. Hodych (1997), Comparing remanence anisotropy and susceptibility anisotropy as predictors of paleomagnetic inclination shallowing in turbidites from the Scotian Rise, *Phys. Chem. Earth*, *22*(1–2), 189–193.

Bragin, V., V. Reutsky, K. Litasov, V. Malkovets, A. Travin, and D. Mitrokhin (1999), Paleomagnetism and $Ar^{40}/^{39}Ar$-dating of late Mesozoic volcanic pipes of Minusinsk depression (Russia), *Phys. Chem. Earth*, *24*(6), 545–549.

Chan, L. (1991), Paleomagnetism of Late Mesozoic granitic intrusions in Hong Kong: Implications for Upper Cretaceous reference pole of south China, *J. Geophys. Res.*, *96*, 327–335.

Chauvin, A., R. Perroud, and M. L. Bazhenov (1996), Anomalous low Paleomagnetic inclination from Oligocene-lower Miocene red beds of the south-west Tien Shan, central Asia, *Geophys. J. Int.*, *126*, 303–313.

Chen, Y., et al. (1991), Paleomagnetic study of Mesozoic continental sediments along the northern Tienshan (China) and heterogeneous strain in central Asia, *J. Geophys. Res.*, *96*, 4062–4082.

Chen, Y., J.-P. Cogné, and V. Courtillot (1992), New paleomagnetic poles from the Tarim Basin, northwestern China, *Earth Planet. Sci. Lett.*, *114*, 17–38.

Chen, Y., S. Gilder, N. Halim, J. Cogné, and V. Courtillot (2002), New paleomagnetic constraints on central Asian kinematics: Displacement along the Altyn Tagh fault and rotation of the Qaidam Basin, *Tectonics*, *21*(5), 1042, doi:10.1029/2001TC901030.

Cogné, J. P., N. Halim, Y. Chen, and V. Courtillot (1999), Resolving the problem of shallow magnetizations of Tertiary age in Asia: Insights from paleomagnetic data from the Qiangtang, Kunlun, and Qaidam blocks (Tibet, China), and a new hypothesis, *J. Geophys. Res.*, *104*, 17,715–17,734.

Dewey, J. F., S. Cande, and W. C. Pitman III (1989), Tectonic evolution of the India/Eurasia collision zone, *Eclogae Geol. Helv.*, *82*, 717–734.

Enkin, R., V. Courtillot, L. Xing, Z. Zhang, Z. Zhuang, and J. Zhang (1991), The stationary Cretaceous paleomagnetic pole of Sichuan (South China Block), *Tectonics*, *10*, 547–559.

Fisher, R. A. (1953), Dispersion on a sphere, *Proc. R. Soc London., Ser. A*, *217*, 295–305.

Funahara, F., N. Nishiwaki, M. Miki, F. Murata, Y. Otofuji, and Y. Wang (1992), Paleomagnetic study of Cretaceous rocks from the Yangtze block, central Yunnan, China: Implications for the India-Asia collision, *Earth Planet Sci. Lett.*, *113*, 77–91.

Ge, T., G. Liu, L. Fang, S. Zhong, N. Wu, V. Hsu, and A. Baksi (1994), Magnetostratigraphic study of the red beds in the Hengyang basin (in Chinese), *Acta Geol. Sin.*, *68*, 379–387.

Gilder, S., and V. Courtillot (1997), Timing of the north-south China collision from new middle to late Mesozoic paleomagnetic data from the North China Block, *J. Geophys. Res.*, *102*, 17,713–17,727.

Gilder, S., R. S. Coe, H. Wu, G. Kuang, X. X. Zhao, Q. Wu, and X. Tang (1993), Cretaceous and Tertiary paleomagnetic results from southeast China and their tectonic implications, *Earth Planet. Sci. Lett.*, *117*, 637–652.

Gilder, S. A., X. X. Zhao, R. S. Coe, Z. F. Meng, V. Courtillot, and J. Besse (1996), Paleomagnetism, tectonics and geology of the southern Tarim basin, northwestern China, *J. Geophys. Res.*, *101*, 22,015–22,031.

Gilder, S., P. Leloup, V. Courtillot, Y. Chen, R. Coe, X. Zhao, W. Xiao, N. Halim, J.-P. Cogné, and R. Zhu (1999), Tectonic evolution of the Tancheng-Lujiang (Tan-Lu) fault via Middle Triassic to Early Cenozoic paleomagnetic data, *J. Geophys. Res.*, *104*, 15,365–15,390.

Gilder, S., Y. Chen, and S. Sen (2001), Oligo-Miocene magnetostratigraphy and rock magnetism of the Xishuigou section, Subei (Gansu Province, western China) and implications for shallow inclinations in central Asia, *J. Geophys. Res.*, *106*, 30,505–30,525.

Gilder, S., Y. Chen, J. P. Cogné, X. Tan, V. Courtillot, D. Sun, and Y. Li (2003), Paleomagnetism of Upper Jurassic to Lower Cretaceous volcanic and sedimentary rocks from the western Tarim Basin and implications for inclination shallowing and absolute dating of the M-0 (ISEA ?) chron, *Earth Planet. Sci. Lett.*, *206*, 587–600.

Halim, N., J.-P. Cogné, Y. Chen, R. Atasiei, J. Besse, V. Courtillot, S. Gilder, J. Marcoux, and R. Zhao (1998), New Cretaceous and Early Tertiary paleomagnetic results from Xining-Lanzhou basin, Kunlun and

Qiangtang blocks, China: Implications on the geodynamic evolution of Asia, *J. Geophys. Res.*, *103*, 21,025–21,045.
Hankard, F., J. Cogné, and V. Kravchinsky (2003), New Tertiary and Cretaceous paleomagnetic poles from Monlonia: Implications on deformation of Eurasia, paper presented at EGS-AGU-EUG Joint assembly, Nice, France.
Hunan Bureau of Geology and Mineral Resources (HBGMR) (1992), *Regional Geology of Hunan Province* (in Chinese), Geol. Publ. House, Beijing.
Hodych, J. P., and K. L. Buchan (1994), Early Silurian palaeolatitude of the Springdale Group red beds of central Newfoundland: A palaeomagnetic determination with a remanence anisotropy test for inclination error, *Geophys. J. Int.*, *117*, 640–652.
Hsu, V. (1987), Paleomagnetic results from one of the red basins in south China, *Eos Trans. AGU*, *68*, 295.
Huang, K., and N. Opdyke (1992), Paleomagnetism of Lower Cretaceous to Lower Tertiary rocks from southwestern Sichuan: A revisit, *Earth Planet. Sci. Lett.*, *112*, 29–40.
Kent, D., and M. Smethurst (1998), Shallow bias of paleomagentic inclinations in the Paleozoic and Precambrian, *Earth Planet. Sci. Lett.*, *160*, 391–402.
Kent, D. V., G. Xu, K. Huang, W. Y. Zhang, and N. D. Opdyke (1986), Widespread late Mesozoic to recent remagnetization of Paleozoic and Lower Triassic sedimentary rocks from south China, *Tectonophysics*, *139*, 133–143.
Kirschvink, J. L. (1980), The least-squares line and plane and analysis of paleomagnetic data, *Geophys. J. R. Astron. Soc.*, *62*, 699–718.
Kodama, K. P., and W. W. Sun (1992), Magnetic anisotropy as a correction for compaction-caused paleomagentic inclination shallowing, *Geophys. J. Int.*, *111*, 465–469.
Li, Y., Z. Zhang, M. McWilliams, R. Sharps, Y. Zhai, Y. Li, Q. Li, and A. Cox (1988), Mesozoic paleomagnetic results of the Tarim craton: Tertiary relative motion between China and Siberia, *Geophys. Res. Lett.*, *15*, 217–220.
Li, Z., I. Metcalfe, and X. Wang (1995), Vertical-axis bock rotations in southwestern China since the Cretaceous: New paleomagnetic results from Hainan Island, *Geophys. Res. Lett.*, *22*, 3071–3074.
Lin, J., M. Fuller, and W. Zhang (1985), The apparent polar wander paths for the north and south China blocks, *Nature*, *313*, 444–449.
Lin, W., Y. Chen, M. Faure, and Q. Wang (2003), Tectonic implications of new Late Cretaceous paleomagnetic constraints from eastern Liaoning Peninsula, NE China, *J. Geophys. Res.*, *108*(B6), 2313, doi:10.1029/2002JB002169.
Liu, Y., and H. Morinaga (1999), Cretaceous paleomagnetic results from Hainan Island in south China supporting the extrusion model of Southeast Asia, *Tectonophysics*, *301*, 133–144.
Lowrie, W. (1990), Identification of ferromagnetic minerals in a rock by coercivity and unblocking temperature properties, *Geophys. Res. Lett.*, *17*, 159–162.
Ma, X., Z. Yang, and L. Xing (1993), The lower Cretaceous reference pole from north China, and its tectonic implications, *Geophys. J. Int.*, *115*, 323–331.
McFadden, P. L., and M. W. McElhinny (1990), Classification of the reversals test in paleomagnetism, *Geophys. J. Int.*, *130*, 725–729.
Michona, L., R. Balenb, O. Merlec, and H. Pagnier (2003), The Cenozoic evolution of the Roer Valley Rift System integrated at a European scale, *Tectonophysics*, *367*, 101–126.
Morinaga, H., and Y. Liu (2004), Cretaceous paleomagnetism of the eastern South China Block: Establishment of the stable body of SCB, *Earth Planet. Sci. Lett.*, *222*, 971–988.
Ojha, T. P., R. F. Butler, J. Quade, P. G. Decelles, D. Richards, and B. N. Upreti (2000), Magnetic polarity stratigraphy of the Neogene Siwalilk Group at Khutia Khola, far western Nepal, *Geol. Soc. Am. Bull.*, *112*, 424–434.
Otofuji, Y., Y. Liu, Yokohama, M. Tamai, and J. Yin (1998), Tectonic deformation of the southwestern part of the Yangtze craton inferred from paleomagnetism, *Earth Planet. Sci. Lett.*, *156*, 47–60.
Robert, A. P., Y. Cui, and K. L. Verosub (1995), Wasp-waisted hysteresis loop: Mineral magnetic characteristics and discrimination of components in mixed magnetic systems, *J. Geophys. Res.*, *100*, 17,909–17,924.
Sato, K., Y. Liu, Z. Zhu, Z. Yang, and Y. Otofuji (2001), Tertiary paleomagnetic data from northwestern Yunnan, China: Further evidence for large clockwise rotation of the Indochina block and its tectonic implications, *Earth Planet. Sci. Lett.*, *185*, 185–198.
Sewell, R. J., S. D. G. Campbell, and D. W. Davis (1998), Three new U-Pb ages from igneous rocks in the new territories of Hong Kong and their structural significance, *Hong Kong Geol.*, *4*, 31–36.
Si, J., and R. Van der Voo (2001), Too-low magnetic inclinations in central Asia: An indication of a long-term Tertiary non-dipole field?, *Terra Nova*, *13*(6), 471–478.
Tamai, M., Y. Otofuji, Y. Lu, and Y. Liu (1996), Paleomagnetic study of Cretaceous rocks from Xichang, southwestern Sichuan, China: Areal extent of tectonic stiffness for the Yangtze block, paper presented at 30th International Geological Congress, Beijing, China.
Tan, X., K. P. Kodama, and D. Fang (1996), A preliminary study of the effect of compaction on the inclination of the redeposited haematite-bearing sediments disaggregated from Eocene redbeds (Suweiyi Fm) from the Tarim basin, northwest China, *Eos Trans AGU*, *77*(46), Fall Meet. Suppl., F155.
Tan, X., K. P. Kodama, H. Chen, D. Fang, D. Sun, and Y. Li (2003), Paleomagnetism and magnetic anisotropy of Cretaceous red beds from the Tarim basin, northwest China: Evidence for a rock magnetic cause of anomalously shallow paleomagnetic inclinations from central Asia, *J. Geophys. Res.*, *108*(B2), 2107, doi:10.1029/2001JB001608.
Tapponnier, P., G. Peltzer, R. Armijo, A. La Dain, and P. Cobbold (1982), Propagating extrusion tectonics in Asia: New insights from simple experiments with plasticine, *Geology*, *10*, 611–616.
Thomas, J., H. Perroud, P. R. Cobbold, M. L. Bazhenov, V. S. Burtman, A. Chauvin, and E. Sadybokasov (1993), A paleomagnetic study of Tertiary formations from the Kyrgyz Tien Shan and its tectonic implications, *J. Geophys. Res.*, *98*, 9571–9589.
Trifonov, V. (2004), Active faults in Eurasia: General remarks, *Tectonophysics*, *380*, 123–130.
Watson, G. S., and R. J. Enkin (1993), The fold test in paleomagnetism as a parameter estimation problem, *Geophys. Res. Lett.*, *20*, 2135–2137.
Yang, Z., and J. Besse (1993), Paleomagnetic study on Permian and Mesozoic sedimentary rocks from north Thailand supports the extrusion model for Indochina, *Earth Planet. Sci. Lett.*, *117*, 525–552.
Yang, Z., and J. Besse (2001), New Mesozoic apparent polar wander path for south China: Tectonic consequences, *J. Geophys. Res.*, *106*, 8493–8520.
Yang, Z., V. Courtillot, and J. Besse (1992), Jurassic paleomagnetic constraint on the collision of the North and South China blocks, *Geophys. Res. Lett.*, *19*, 577–580.
Yang, Z. Y., J. Y. Yin, Z. M. Sun, Y. Otofuji, and K. Sato (2001), Discrepancy Cretaceous paleomagnetic poles between eastern China and Indochina: A consequence of the extrusion of Indochina, *Tectonophysics*, *334*, 101–113.
Yegorova, T. P., and V. Starostenko (1999), Large-scale three-dimensional gravity analysis of the lithosphere below the transition zone from western Europe to the East European Platform, *Tectonophysics*, *314*, 83–100.
Yoshioka, S., Y. Liu, K. Satoa, H. Inokuchic, L. Su, H. Zamana, and Y. Otofujia (2003), Paleomagnetic evidence for post-Cretaceous internal deformation of the Chuan Dian Fragment in the Yangtze block: A consequence of indentation of India into Asia, *Tectonophysics*, *376*, 61–74.
Zhai, Y., M. K. Seguin, Y. Zhou, J. Dong, and Y. Zheng (1992), New paleomagnetic data from the Hunan Block, China, and Cretaceous tectonics in eastern China, *Phys. Earth Planet Inter.*, *73*, 163–188.
Zhao, X., R. Coe, Y. Zhou, S. Hu, H. Wu, G. Kuang, Z. Dong, and J. Wang (1994), Tertiary paleomagnetism of north and south China and a reappraisal of late Mesozoic paleomagnetic data from Eurasia: Implications for the Cenozoic tectonic history of Asia, *Tectonophysics*, *235*, 181–235.
Zhao, X., P. Riisager, J. Riisager, U. Draeger, R. Coea, and Z. Zheng (2004), New palaeointensity results from Cretaceous basalt of Inner Mongolia, China, *Phys. Earth Planet Inter.*, *141*, 131–140.
Zheng, Z., M. Kono, H. Tsunakawa, G. Kimura, Q. Wei, X. Zhu, and T. Hao (1991), The apparent polar wander path for the north block since the Jurassic, *Geophys. J. Int.*, *104*, 29–40.
Zheng, Z., H. Tanaka, Y. Tatsumi, and M. Kono (2002), Basalt platforms in Inner Mongolia and Hebei Province, northeastern China: New K–Ar ages, geochemistries and revision of palaeomagnetic results, *Geophys. J. Int.*, *151*, 654–662.

J. Pei and Z. Sun, Laboratory of Paleomagnetism, Institute of Geomechanics, CAGS, Beijing, China 100081. (sunzm1209@yahoo.com.cn)

T. Yang, Institute of Tibetan Plateau Research, Chinese Academy of Science, Beijing, China 100085.

Z. Yang, Department of Earth Sciences, Nanjing University, Nanjing, China 210093.

Q. Yu, Department of Geophysics and Geoinformation Systems, China University of Geosciences, Beijing, China 100083.